Plasmonic-Nanopore Biosensors for Superior Single-Molecule Detection

Joshua D. Spitzberg, Adam Zrehen, Xander F. van Kooten, and Amit Meller*

Plasmonic and nanopore sensors have separately received much attention for achieving single-molecule precision. A plasmonic "hotspot" confines and enhances optical excitation at the nanometer length scale sufficient to optically detect surface–analyte interactions. A nanopore biosensor actively funnels and threads analytes through a molecular-scale aperture, wherein they are interrogated by electrical or optical means. Recently, solid-state plasmonic and nanopore structures have been integrated within monolithic devices that address fundamental challenges in each of the individual sensing methods and offer complimentary improvements in overall single-molecule sensitivity, detection rates, dwell time and scalability. Here, the physical phenomena and sensing principles of plasmonic and nanopore sensing are summarized to highlight the novel complementarity in dovetailing these techniques for vastly improved single-molecule sensing. A literature review of recent plasmonic nanopore devices is then presented to delineate methods for solid-state fabrication of a range of hybrid device formats, evaluate the progress and challenges in the detection of unlabeled and labeled analyte, and assess the impact and utility of localized plasmonic heating. Finally, future directions and applications inspired by the present state of the art are discussed.

1. Introduction

Sensing single molecules is the ultimate goal of chemical and biochemical analyses. The shift from bulk to single-molecule, wherein each molecule's observation is an independent event, reveals information often intrinsically masked by ensemble measurements, such as sample heterogeneity, molecular mechanisms, and complex kinetic rates. Furthermore, reducing the sample volume and concentration to the minimum possible enables direct and unbiased observation of analytes that otherwise require or do not readily allow direct enzymatic amplifications, such as RNAs and proteins. This precision is important for a broad range of biomedical applications, particularly in cases where multiplexing (the ability to target multiple

J. D. Spitzberg, A. Zrehen, Dr. X. F. van Kooten, Prof. A. Meller
Department of Biomedical Engineering
Technion—IIT
Haifa 32000, Israel
E-mail: ameller@technion.ac.il
Prof. A. Meller
Department of Biomedical Engineering
Boston University
Boston, MA 02215, USA

The ORCID identification number(s) for the author(s) of this article can be found under https://doi.org/10.1002/adma.201900422.

bio-markers simultaneously) is necessary. Finally, single-molecule sensing could simplify the sample workflow, hence reducing cost per sample, while streamlining the integration to bedside monitoring systems and precision medicine.[1]

Clinically relevant biomarker concentrations span over a dozen orders of magnitude,[2,3] from homeostatic proteins (abundant), to trace cytokines (a few per cell), and pathogenic targets (a few in several mL of clinical sample, **Figure 1**). At the lower end of the concentration range, relevant targets include those from bacterial infections such as tuberculosis (TB) and urinary tract infection (UTI), viral infections such as hepatitis C (HCV) and human immunodeficiency virus (HIV), as well as biomarkers for cancer such as circulating nucleic acids (cNAs) and circulating tumor cells (CTCs).

The concentration of targets strongly affects the detection rate of single-molecule sensors. This is particularly true for sensing methods that rely on diffusion to bring analytes to the sensing region. The observation rate (the rate at which molecules encounter the sensor) of freely diffusing analytes is inversely proportional to their concentration, requiring prohibitively long observation times for statistical confidence. On the other hand, at high analyte concentrations the sensing region must be spatially confined to ensure single-molecule occupancy, but a reduction of the sensing volume also reduces the dwell time of the molecule in the sensing zone ($\tau_D \sim V^{\frac{2}{3}}$), thus severely restricting the signal integration time.

Optical detection, in particular fluorescence, is widely used for single-molecule sensing as it allows parallel, multiplexed detection at compatible length scales. Various approaches for enhancing optical detection have been reported involving spatial confinement of the electromagnetic field. These approaches include "structure-less" total internal reflection fluorescence (TIRF) configurations, physically confined zero-mode waveguide (ZMW) apertures, near-field scanning optical microscope (NSOM) probes and a variety of nanoantennae.[4] To obtain single-molecule sensing at a concentration of 100×10^{-9} M, the sensing volume must be smaller than roughly 10 attoliters (10^{-17} L), which is nearly the diffraction limited spot volume of a tightly focused laser beam (of visible wavelength) or the practical volume observed in TIRF illumination. At the other extreme, the detection volume of a highly localized plasmonic structure (e.g., an "antenna-in-a-box' or a bowtie antenna) is just $\approx 10^{-20}$ L.[5] Such volumes are limited by diffusion to high

**ADVANCED
SCIENCE NEWS**
www.advancedsciencenews.com

**ADVANCED
MATERIALS**
www.advmat.de

concentrations (roughly μM or more) to ensure the presence of at least one molecule inside the sensing volume. However, clinically relevant concentrations are often much smaller, sometimes as low as ≈1 × 10^{-15} M or less (Figure 1), thus severely restricting the practical applicability of small plasmonic structures.

Over the past few decades, plasmonic sensors and nanoscale pores ("nanopores") have separately received much attention for achieving single-molecule precision of bound and unbound analytes.[3,6–12] Plasmonic antennae convert far-field optical radiation into localized electromagnetic energy and vice versa,[13] by exploiting the optical properties of metal-dielectric boundaries to generate surface-bound electron oscillations, called plasmons, with an energy density several orders of magnitude larger than that of the incident radiation.[14] The material and geometry of the interface can be designed to maximize the plasmon modal confinement and resonance[15–17] for a gain in signal-to-background ratio (SBR) sufficient to detect resonant shifts, fluorescence emission[9] and Raman scattering spectra[18] induced by the interaction of molecules with a plasmonic "hotspot." The flux of emitted and scattered photons increases with the optical excitation, thus improving the temporal resolution and the SBR. Although nonradiative quenching inherent to metals can result in significant dissipative energy loss,[19] localized heating can also provide beneficial effects, as will be discussed later.

Nanopore sensors are based on nanoscale apertures through which ions can cross an electrically insulating membrane.[20] Solid-state nanopores are commonly defined as nanopores fabricated in synthetic materials, as opposed to biological pores. A voltage bias applied across the membrane actively funnels and threads[21] molecules through the aperture, causing them to interact with the membrane and displace ions within the pore. This displacement is detectable as a change in the ionic current.[22,23] The combination of event amplitude (magnitude of the current blockage) and dwell time (duration of the blockage) is a distinct signature of an unlabeled molecule.[24–26] This "resistive pulse sensing" method has been extended to the detection of molecules barcoded with bulky groups,[27,28] and quenched fluorophores that "unzip" during translocation.[29]

This progress report highlights two fundamental features of nanopore biosensors that are used to overcome challenges associated with sensing freely diffusing analytes. First, the electrical potential gradient in the vicinity of the nanopore actively funnels charged molecules such as nucleic acids and proteins toward the pore's aperture, from distances much longer than the Debye screening length.[21] This active transport enables single-molecule sensing at lower concentrations compared to passive diffusion. Second, the typical nanopore diameter is fabricated to be just slightly larger than the cross-section of the molecule, ensuring serial occupancy of the sensing volume while also constraining the motion of the molecules to one dimension. This confinement enables single-molecule sensing with increased dwell times at a wide range of concentrations. Threading through the pore also linearizes polymer species, allowing sequential observation of sub-molecular sequences.

When the pore is just slightly larger than the cross-section of the analyte, the conditions for single-file translocation through a pore are best ensured. This report therefore focuses

Joshua Spitzberg is conducting his Ph.D. studies in the laboratory of Prof. Amit Meller, in the Department of Biomedical Engineering at the Technion—Israel Institute of Technology, Haifa, Israel. His research aim is modular integration of nanopores systems with optical and microfluidic technologies. His current research interests include single molecule sensing, nano-optics and microfluidics, and creating new tools enabling scalable diagnostic platforms.

Xander van Kooten received his bachelor's degree in electrical engineering from Delft University of Technology (The Netherlands) and his master's degree in electrical engineering from École Polytechnique Fédérale de Lausanne (Switzerland). He completed his Ph.D. as a Marie Curie fellow, jointly between the Technion—Israel Institute of Technology (Haifa, Israel) and IBM Research—Zurich (Switzerland). During his Ph.D. he developed microfluidic electrokinetic methods to enhance the sensitivity of biomolecular assays. His research interests include single-molecule sensing, electrophoresis, and nanofabrication applied to medical diagnostics.
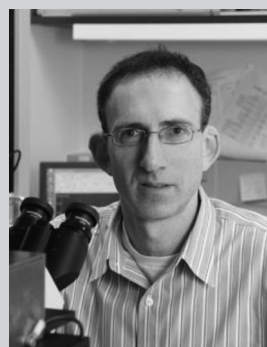
Amit Meller is the Roy Matas Winnipeg Chair in Biomedical Engineering and full professor in the Department of Biomedical Engineering at the Technion—Israel Institute of Technology, Haifa, Israel. He is also director of the Israeli Center of Excellence in Biological Physics (i-Core). He began working on nanopore biosensors in the early days of the field at Harvard University around 1998. Later his lab developed single-molecule electro-optical sensing in nanopores and used it in various applications ranging from sensing DNA epigenetic modifications to proteins. His current research interests include single-molecule sensing and single molecule biophysics, bio-optics, nanosciences, and nano-biotechnology.

**ADVANCED
SCIENCE NEWS**

www.advancedsciencenews.com

**ADVANCED
MATERIALS**

www.advmat.de
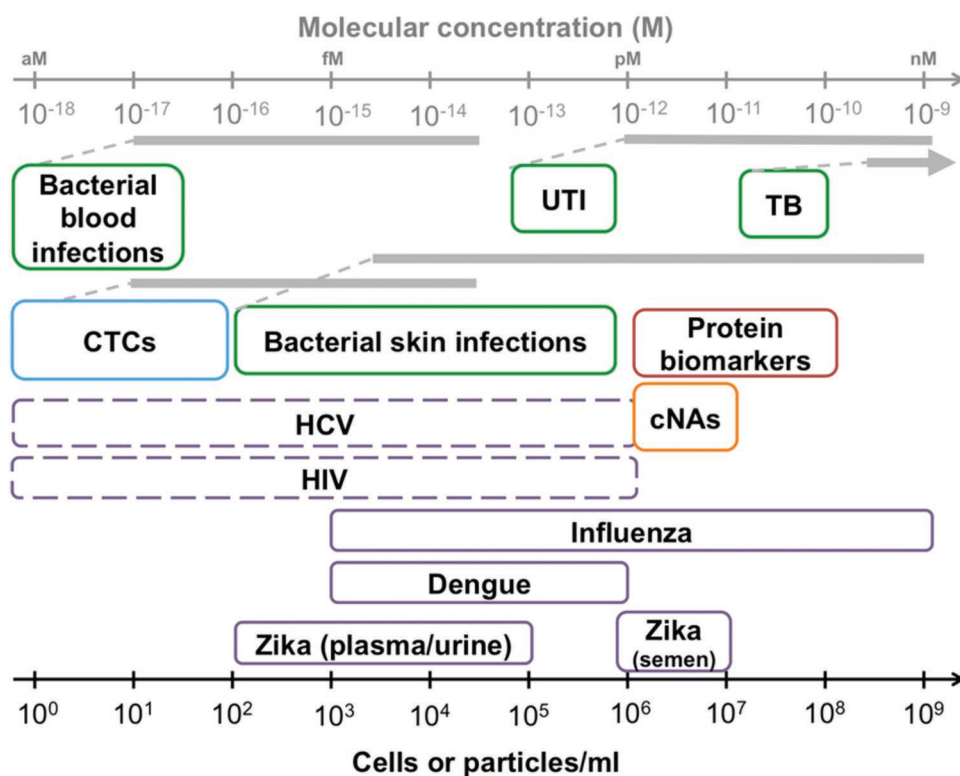
Figure 1. Summary of concentrations of biomolecular analytes in clinical samples. Applications of bacterial detection are outlined in green, viral targets are outlined in purple (with a dotted line for indications where quantitative monitoring is required), and cancer biomarkers are shown in blue (circulating tumor cells), red (protein biomarkers), and orange (circulating nucleic acids). Reproduced with permission.[2] Copyright 2017, American Chemical Society.

on progress in plasmonic nanopore devices with nanometric (<10 nm) pores, in order to provide robust single-molecule sensing and threading of nucleic acids and proteins (cross sections on the order of 1 nm). Furthermore, "small" nanopores can be used to analyze clinically relevant biomarkers extracted from larger objects such as viruses (tens of nm), bacteria, and CTCs (micrometer-scale) as shown in Figure 1. Examples presented below focus on the detection of DNA molecules.

Recently, plasmonic and solid-state nanopore structures have been monolithically integrated to offer complimentary improvements in sensitivity, specificity, observation rate, dwell time, and scalable parallelized detection. Fabrication methods discussed in Section 2 enable co-localization of the surface-bound plasmonic "hotspot," whose structured metal-dielectric interface provides enhanced optical excitation within a sub-diffraction-limited volume, with a nanopore whose molecule-sized aperture actively funnels and interrogates analytes in an intrinsically serial and linearized fashion. Plasmonic nanopores (PNPs) thus offer several important advantages: the ability to measure Raman spectra of single unlabeled analytes, discussed in Section 3, improved spatiotemporal resolution and enhanced signal-to-background of fluorescently labeled analytes, discussed in Section 4, and plasmonic-based heating discussed in Section 5. Notably, both PNP-enhanced Raman scattering and enhanced fluorescence sensing improve specificity via optical fingerprinting. This combination of traits offers significant

potential for fundamental studies in biophysical science as well as for biotechnology applications.

1.1. Plasmonic Sensing

Plasmons are surface-bound charge-density oscillations of the free electron gas of a metal at the interface with a dielectric material.[14] Optically driven displacement of the electron gas with respect to this boundary creates a restoring force between the negatively charged electron gas and the positively charged ion lattice, which in turn generates strong optical near-fields at the interface. The effect is resonant in origin, with the amplitude accumulating over each optical cycle, while simultaneously experiencing dampening due to Ohmic losses in the metal and other mechanisms.[30] The development of plasmonic sensors is centered on designing structures to achieve maximum modal confinement and concentration of electromagnetic energy, to sufficiently enhance the strength of surface–analyte interactions for single-molecule sensitivity at high spatiotemporal resolution. Although Maxwell's equations are scale invariant, material properties are spectrally dependent, which limits the range of electromagnetic frequencies and materials that support plasma oscillations. For this reason, gold and silver are commonly chosen for devices active in the visible spectrum, and the development of materials with varied resonance features and reduced loss is an active area of research.[31,32] Reshaping the

ADVANCED
SCIENCE NEWS
www.advancedsciencenews.com

ADVANCED
MATERIALS
www.advmat.de

metal–dielectric interface shifts the resonant frequency of the structure and alters the plasmon's intensity.[15,17] For example, mode confinement at a "sharp" boundary feature, such as a tip, particle, or gap, may lead to significant optical near-field amplification and localization.[33] Similarly, changes in the dielectric properties at the interface, such as those caused by molecular analytes, may also lead to enhancement. This forms the basis of label-free plasmon resonance sensing of single molecules.

Development of plasmonic nanoantennae is an extremely active field. Fabrication techniques range from top-down to bottom-up,[34] and approaches to optimizing mode confinement and resonance spectra involve both deterministic[35–38] and generative methods.[39–41] This has led to a variety of implementations of single-molecule fluorescence enhancement strategies. Computational simulation is heavily employed to systematically explore the geometric and material parameter space for even geometrically simple structures.[17,42] Nevertheless, it remains essential to experimentally confirm predictions and to update models based on real fabrication profiles,[43] as even sub-nanometric variations in fabrication can have significant consequences at these length scales.[44,45]

Plasmonic devices have primarily been employed in three sensing modes: refractometric, surface-enhanced Raman spectroscopy, and fluorescence emission. In each case the confined electromagnetic field mediates plasmon–molecule interactions to enhance optical sensing (**Figure 2**). Refractometric sensing is the simplest, and most common configuration. Molecules binding to a surface cause an increase in the local refractive index,[46,47] leading to a shift in plasmon resonance (Figure 2, panel III, bottom). This approach is limited in sensitivity by the nonspecific adsorption of analytes to the surface. Although the sensitivity can be increased by using an enzyme-linked immunosorbent assay (ELISA) to increase the apparent affinity of analytes[48] or by using surface coatings to reduce nonspecific adsorption, both of these approaches require *a priori* knowledge of the target analyte. A further limitation of resonance-shift sensing is that the change in refractive index depends on the

location and orientation of the molecule with respect to the plasmonic hotspot. This results in a stochastic distribution of the detected signal,[49,50] which can only be reduced by spatially controlling the binding of analytes to the surface.

The second sensing modality, Raman spectroscopy, is based on detecting the characteristic vibrational states of molecular bonds. Although rich structural information can be deduced from Raman spectra of unlabeled molecules, obtaining such information is practically challenging, as the Raman cross-section is often 12–14 orders of magnitude smaller than typical fluorescence cross-sections.[51] Surface-enhanced Raman spectroscopy (SERS), in which the Raman signal of analytes is enhanced in the vicinity of "rough" metal surfaces, provides a way to overcome this. Electromagnetic and chemical effects at metal surfaces enhance the interaction, although the exact mechanisms are a continuing subject of investigation. First, plasmon hotspots increase the density of states at the Stokes-shifted wavelength. An analyte within this plasmonic hotspot exhibits enhanced amplitude of Raman scattering, similar to the schematic configuration of Figure 2 (panel III, top). Second, "chemical" enhancement arises from changes in molecular state due to surface–analyte interactions. Plasmonics is a powerful approach for enhancing SERS, as the strength of the Raman scattering interaction scales with the fourth power of the electric field. Overall enhancement factors on the order of 10^{14} have been reported for roughened metallic surfaces,[18] yet deterministic formation of hotspots and active delivery of analytes to these sites remains an open challenge. As enhancement factors are not uniform across SERS substrates, molecules must be consistently positioned near hotspots to improve the Raman signal.

In addition to detecting analytes using resonance shift sensing and Raman spectroscopy, plasmonic sensors can be designed to minimize fluorescence quenching and to maximize the enhancement of the incident field, thus allowing single fluorescent molecules to be resolved. Fluorescence emission scales as the product of excitation and quantum yield,[52] allowing
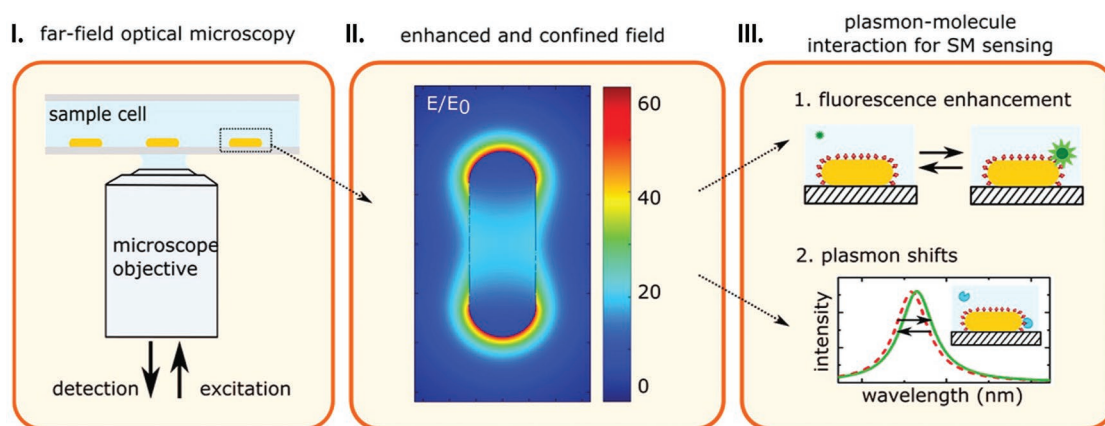
Figure 2. Principle of plasmon-enhanced single-molecule sensing using nanoparticles. I) The sensor (yellow rod) is typically probed using an optical microscope. II) The plasmon resonance induces a strongly enhanced and tightly confined electromagnetic field around the particles. The field shown here is for a gold nanorod that is excited at its resonant frequency calculated using the boundary element method. III) This local field mediates plasmon–molecule interactions, enabling enhanced single-molecule detection by monitoring plasmon-induced changes of the molecule (resulting in, e.g., enhanced fluorescence or enhanced Raman scattering) or by monitoring molecule-induced changes of the plasmon (resulting in frequency shifts of the plasmon). Adapted with permission.[3] Copyright 2017, American Chemical Society.
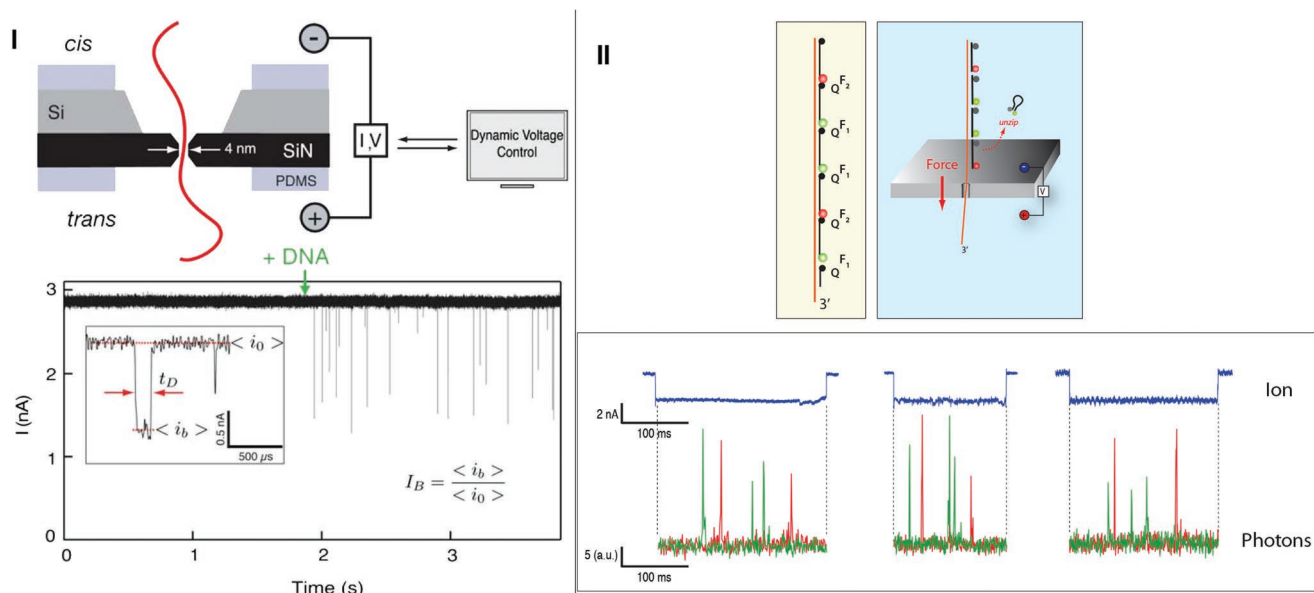
Figure 3. I) Nanopore-based electrical sensing. Top: schematic illustration of a solid-state nanopore device for probing DNA translocation dynamics (not to scale). DNA molecules are driven through the nanopore by an applied voltage while the ionic current is measured. Bottom: typical ionic current trace for a 4 nm pore, before and after the introduction of 5×10^{-9} M 400 bp DNA to the *cis* chamber (green arrow). The transient current-blockade events correspond to single-molecule translocation of DNA. The inset displays a magnified translocation event in which the relevant parameters used in this article are defined. Adapted with permission.[63] Copyright 2008, Biophysical Society. II) Electro-optical sensing of DNA "barcodes." High SBR measurements of two-color DNA barcodes. Top: single-stranded DNA template harboring 16-mer binding sequences for five molecular beacons, labeled with a unique sequence of green and red fluorophores (F1 and F2, respectively), and a schematic illustration of the nanopore beacon unzipping setup. Bottom: typical unzipping events using a low photoluminescence 3 nm pore, where optical and electrical signals are measured simultaneously, showing five clear photon bursts per event in the green and red channels, in accordance with the DNA templates. Adapted with permission.[64] Copyright 2015, American Chemical Society.

significant enhancement within a plasmonic hotspot (Figure 2, panel III, top). While excitation enhancements on the order of 10^4 are not uncommon, these typically occur within metal–dielectric–metal gaps approaching less than 10 nm separation in which quenching reduces the overall emission.[53] Quenching refers to nonradiative energy transfer processes that lead to reduced fluorescence emission in the vicinity of metal surfaces, including ohmic losses. Strategies to counter quenching include depositing a thin polymer layer on the metal surface to act as a spacer between the fluorophore and the surface.[8] The fluorescence enhancement in plasmonic devices can be improved in other ways besides reducing quenching. First, large enhancement factors can be achieved using low-yield fluorophores, as the hotspot provides additional favorable pathways for radiative decay to the ground state, thereby increasing the radiative rate. The enhancement is larger for a low-yield emitter than it is for an ideal emitter, as the latter cannot have a yield larger than unity and therefore benefits less from plasmonic enhancement of emission. Second, fluorophores outside the hotspot can be quenched or, in some cases, shielded from incident light, leading to a suppression of the background fluorescence. Combinations of engineered plasmonic structures with dye quenching has led to demonstrations of fluorescence enhancement factors over 1000-fold for analytes positioned within zeptoliter hotspots.[5,54] In contrast to label-free methods, fluorescence sensing can offer improved specificity and can enable spectral multiplexing, albeit at the cost of increased complexity.

1.2. Nanopore Sensing

Solid-state nanopores (ssNPs) are a type of single-molecule sensor that has been shown to be promising for a variety of biological applications, including nucleic acid sequencing,[55] pathogen typing,[24] protein discrimination[56] and RNA structure analysis.[57] An ssNP device consists of an electrically insulating, ultrathin (a few nanometers) membrane in which a nanometer-scale pore is formed. Electrodes, usually Ag/AgCl, are inserted into electrolyte-filled chambers to apply a voltage across the pore, resulting in an electrophoretic force that attracts charged biomolecules to the pore. As a molecule passes through the pore, it displaces ions, leading to a pico- to nano-ampere change in the current measurement from an "open pore" level i_o to a "blocked pore" level i_b (**Figure 3**, panel I). The combination of the fractional event amplitude $I_B = <i_b/i_o>$ (blockage depth) and event dwell time τ_D (blockage duration) is a molecular signature, which can be used in various sensing applications, for example to identify pathogens from single-nucleotide variations (SNVs)[24] or to decode information by reading a sequence of bulky nucleic acid structures.[28]

The development of nanopore sensing techniques has been largely catalyzed by the quest for novel single-molecule DNA sequencing strategies, following the completion of the human genome project.[58–60] An important step forward in this area took place when a molecular motor enzyme was used to feed a strand of DNA base-by-base through the nanopore while changes in the nanopore's conductance were read,

ADVANCED
SCIENCE NEWS
www.advancedsciencenews.com

ADVANCED
MATERIALS
www.advmat.de

a concept that eventually matured to a commercial sequencing platform.[61] Nevertheless, single-molecule gene sequencing still requires substantial sample preparation as well as samples containing a minimum number of copies, requirements that are incompatible with many biomedical applications. Complementary methods can alleviate the challenge of minimum copy number in cases where genotyping, i.e., identification of a certain known sequence, is the main goal. For instance, sequence-specific molecular tags such as peptide nucleic acids (PNA), locked nucleic acids (LNA) or morpholinos can be used to create unique "barcodes" on the target DNA molecules, enabling nanopore-based identification of single molecules while potentially circumventing the need for conventional amplification techniques such as polymerase chain reaction (PCR).[62]

Several hurdles have yet to be overcome to enable resistive pulse sensing for more sensitive applications; specifically, nonideal noise components,[65,66] insufficient temporal and spatial resolution,[67] and low analyte throughput. Researchers have developed complementary optical tools to enhance the ssNP utility through simultaneous electrical and optical transduction.[22,68–70] Under confocal or total internal reflection (TIR) illumination, an excitation laser beam is directed at the nanopore to excite fluorescently labeled biomolecules. The emitted light is spatially filtered in the case of confocal illumination, and detected by an avalanche photodiodes or a single-photon camera (e.g., EM-CCD). The ability to temporally resolve photon bursts in multiple colors during the passage of a biomolecule through the nanopore greatly extends the scope of nanopore sensing, as it permits a flexible design of combinatorial sets of colored probes for *optical* barcoding. Optical barcoding can provide information that is complimentary and orthogonal to the structural information obtained using *electrical* barcodes. An example of two-color DNA barcode readout using simultaneous electrical and optical sensing is shown in Figure 3 (panel II, top). The sequence of fluorophores uniquely identifies analytes with single-molecule sensitivity. Target DNA is converted according to a binary code, which is recognized by molecular beacons with one of two different fluorophores. The head-to-tail configuration of the hybridized beacons causes the fluorophores to remain quenched, until they are stripped off as the template strand translocates through the narrow pore. This results in a series of detectable photon bursts at high speed. In this way, the two unique capabilities of the nanopore, i) drawing in charged molecules serially and ii) linearizing the molecule, enable single-polymer sensing and analysis of monomeric subunits. This applies equally well to hybrid detection, as demonstrated by the electrical and optical traces in Figure 3 (panel II, bottom). As has been demonstrated, optical signals from multiple nanopores can be stimulated and detected in parallel using a single array sensor, providing a method for straightforward and scalable parallelized sensing by large nanopore arrays.[29]

In conventional resistive-pulse sensing, the presence of multiple nanopores in the same membrane may result in overlapping electric signals that cannot be decoded. This challenge can be overcome by simultaneously recording optical signals from an array of pores. Although implementations of optical sensing have until now employed primarily a single nanopore per device, significant efforts are being made to improve

throughput, with the goal of simultaneous readout of hundreds to thousands of nanopores on a single chip.[22] Optical nanopore sensing has been successfully applied to DNA barcode discrimination[29] mapping of epigenetic modifications,[71] DNA length discrimination[64,72] and polypeptide discrimination.[73]
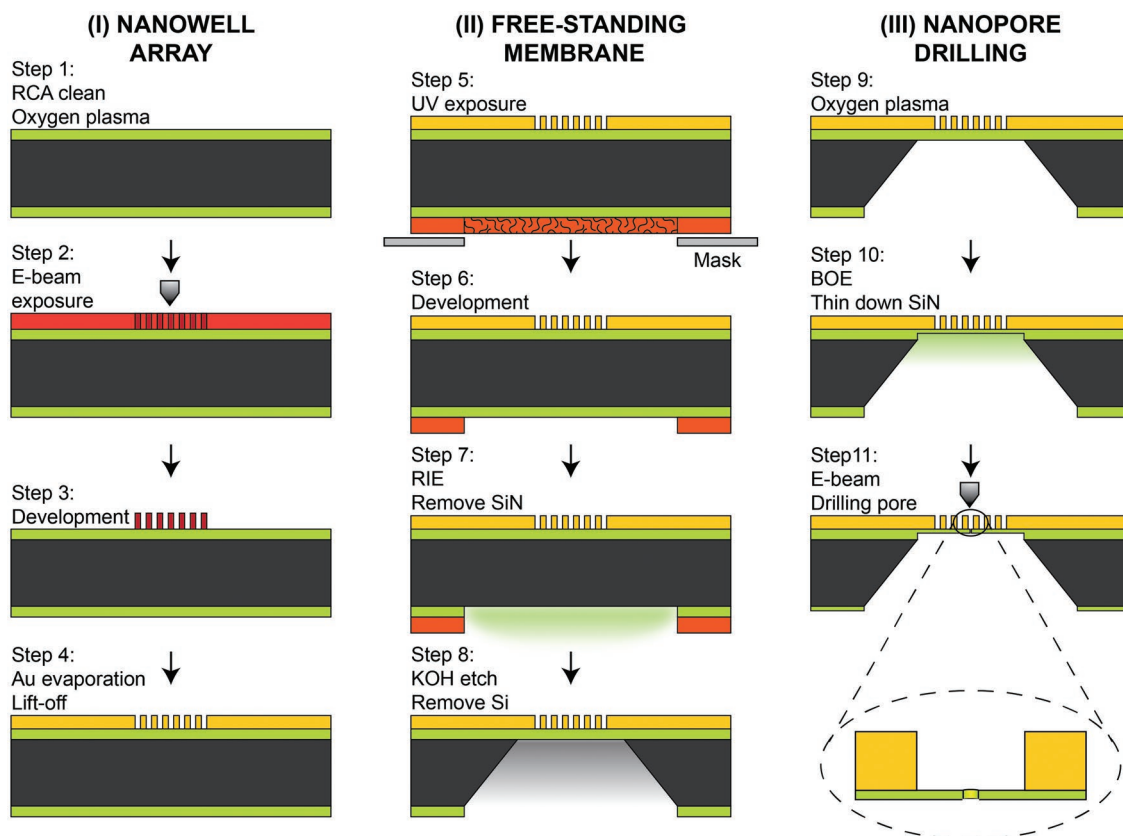
1.3. Plasmonic Nanopores

Several fundamental features of nanopore sensors and plasmonic enhancement make the combination of the two sensing modalities both complimentary and powerful. In plasmonic sensing, the confinement of the electromagnetic field at hotspots mediates and enhances the SBR of plasmon–molecule interactions for improved single-molecule sensing. Although a smaller hotspot is typically associated with a larger amplification of the electromagnetic field, both the arrival time and dwell time of a freely diffusing molecule to and within the hotspot decrease sharply with the hotspot volume, limiting the overall signal integration. Solid-state nanopores can however deliver charged analyte molecules from bulk to a predetermined point in space, and can therefore be used to spatially localize analyte molecules at a plasmonic hotspot. Moreover, a molecule captured in the nanopore is practically restricted to one-dimensional motion; hence, the dwell time can be substantially increased by reducing the diameter of the nanopore.[63] Therefore, both the likelihood of sensing an individual molecule from bulk and the expected signal-to-background ratio are increased in hybrid plasmonic nanopore structures, as compared to either of the methods independently.

2. Fabrication

Fabrication of solid-state plasmonic nanopore devices can be separated into three main processes: i) fabrication of the plasmonic structure, ii) fabrication of the freestanding membrane, and iii) nanopore drilling. Lithography and milling are the two principal methods for constructing architectures supporting plasmonic resonance. Depending on the method employed, either the plasmonic layer or the nanopore layer can be completed first, while nanopore drilling is reserved for the last step. A simpler, though more limited strategy that differs from this format, is to metallize the nanopore itself to achieve a plasmonic effect at the edges of the pore. The freestanding membranes are most commonly prepared by patterning a series of squares with sides on the order of the wafer thickness, using optical lithography, followed by etching of a hard mask, anisotropic wet etching of <100> silicon, with additional etching steps depending on the presence of a noise-insulating layer such as silicon dioxide. We focus on progress in the first (i) and third (iii) steps of plasmonic nanopore fabrication.

2.1. E-Beam Lithography for Constructing Plasmonics

Electron-beam lithography (EBL) is one of the most prevalent techniques for creating high-resolution wafer-scale nanostructures for plasmonic applications. The EBL resolution, dependent on spot size, electron scattering, resist development

**ADVANCED
SCIENCE NEWS**
www.advancedsciencenews.com

**ADVANCED
MATERIALS**
www.advmat.de

**(I) NANOWELL
ARRAY**

Step 1:
RCA clean
Oxygen plasma

Step 2:
E-beam
exposure

Step 3:
Development

Step 4:
Au evaporation
Lift-off

**(II) FREE-STANDING
MEMBRANE**

Step 5:
UV exposure

Mask

Step 6:
Development

Step 7:
RIE
Remove SiN

Step 8:
KOH etch
Remove Si

**(III) NANOPORE
DRILLING**

Step 9:
Oxygen plasma

Step 10:
BOE
Thin down SiN

Step11:
E-beam
Drilling pore

Figure 4. Schematic of wafer-scale fabrication of plasmonic nanowell–nanopore devices using electron-beam lithography to construct the plasmonic architecture. The substrate is $SiN_x/Si/SiN_x$. i) Single-pixel dots were exposed at 30 kV (Raith 150) to define the nanowells. 5 nm Cr and 130 nm Au was deposited by e-beam evaporation, and then lifted off to leave behind an imprint of pillars forming nanowell arrays. ii) To create free-standing membranes, a series of squares were backside-aligned to the nanowells and etched anisotropically with KOH. iii) The 25 nm thick SiN_x membranes were thinned down to 10 nm using buffered oxide etch, to improve the signal-to-noise ratio. Adapted with permission.[76] Copyright 2017, Wiley-VCH.

and other factors,[74] has been lowered to sub-5 nm in isolated feature size and pattern density.[75] To construct plasmonic nanowell–nanopore devices, Assad et al. used a negative tone e-beam process to pattern an array of 120 nm diameter gold nanowells (**Figures 4** and **5**a), at the center of a free-standing silicon nitride (SiN_x) membrane. Briefly, Ma-N 240 resist, which has a resolution down to 50 nm, was spun to a thickness of 300 nm. A pattern of nanowell arrays and alignment marks were defined as single dots using a Raith 150 at 30 kV accelerating voltage, the maximum voltage to prevent failure of the lift-off due to resist overcutting. After immersing in Ma-D 525 developer, the array of cylindrical columns remaining on the wafer served as the nanowell openings. A thin chromium film of 5 nm was then deposited as an adhesion layer, followed by 130 nm of gold. Finally, the resist pillars were removed in Microposit 1165 resist remover.[76]

A similar procedure was used to create two 90 nm long, 30 nm thick gold equilateral triangles (a bowtie-like shape), facing each other with a 1–10 nm gap between the tips (Figure 5b).[77,78] Inverted-bowtie nanoapertures can be created using a trilayer positive resist stack consisting of PMGI/MMA-MAA copolymer/ PMMA, which works at a higher acceleration voltage (100 kV) and allows the gold layer to be stripped away easily.[79] An alternative to lift-off, which is an additive process, is to perform EBL on a metal-coated wafer, followed by isotropic or anisotropic etching. For example, reactive ion etching (RIE) with argon gas was used to open up 200 nm nanoholes in a 50 nm thick gold film,[80] and reactive ion beam etching (RIBE), was used to pattern 20 nm thick 100 nm spaced SERS line gratings.[81]

While EBL is a wafer-scale and therefore high-throughput process, it requires at least two alignment steps, depending on the number of different heights, which adds to processing time and imposes restrictions on structure possibilities. Alignment accuracies vary between sub-10 to 30 nm depending on the sophistication of the alignment procedure and equipment.[82–84] Nanoimprint lithography (NIL) can further increase throughput over EBL since it relies on a single master template instead of write repeats, but this only makes sense in the context of an optimized design for mass production.[85] The ultimate throughput will also be affected by the chosen nanopore drilling technique as outlined in Section 2.4.

2.2. FIB Milling for Constructing Plasmonics

Focused ion beam (FIB) milling is an entirely physical process relying on momentum transfer from the ion beam to the atoms of the substrate. Collisions that have energy greater than the
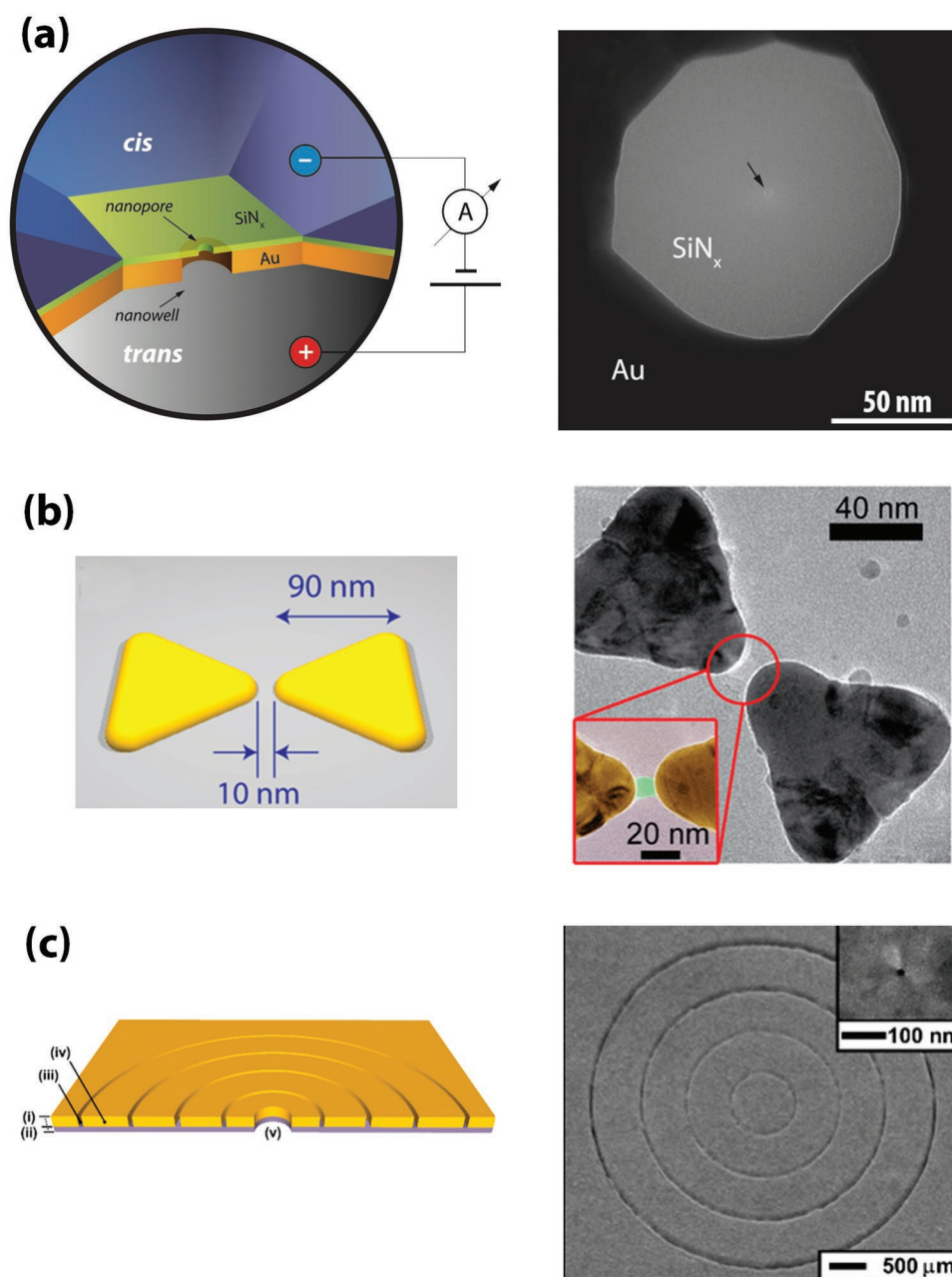
Figure 5. Plasmonic nanopore designs and their fabrication techniques. a) Plasmonic nanowell fabricated by EBL. Left: Free-standing membrane with a gold nanowell. Right: SEM image inside the gold nanowell with an arrow pointing to a TEM-drilled pore. Adapted with permission.[76] Copyright 2017, Wiley-VCH. b) Plasmonic bowtie fabricated by EBL. Left: Schematic of the bowtie structure fabricated from 1 nm Ti and 30 nm Au. Right: TEM image of plasmonic bowtie. Inset shows a false-color zoom in on the gap and nanopore. Adapted with permission.[77] Copyright 2015, American Chemical Society. c) Plasmonic bullseye structure fabricated by FIB. Left: Schematic of the structure where (1) is a 47 nm layer of Au and 3 nm layer of Ti, (2) is a 20 nm thick SiN$_x$ membrane, and (3) is a bullseye ring with a height of ≈80 nm. The pitch between rings (4) is 518 nm, and the nanopore (5) is 20 nm (oversized for visualization). Right: SEM image of the bullseye structure and FIB image of the nanopore structure (inset). Adapted with permission.[89] Copyright 2017, American Chemical Society.

substrate's binding energy (3.8 eV for gold) will result in ejection of the atom, and normally a collision cascade is desirable to increase the sputtering yield or number of atoms removed per incident ion. The yield is typically 1–50 atoms per collision and depends on the mass and energy of incident ions, the mass of target atoms, direction of incidence, target temperature and ion flux. Besides sputtering, the other governing effect controlling the material removal is redeposition, which occurs when a portion of ejected atoms returns to the sputtered region. By fine-tuning the size, shape, current, and energy of the ion beam, it is possible to produce complex pseudo-3-dimensional structures with nanometer precision.[86] FIB milling is superior to EBL for structures with variable and curvilinear heights, such as the "antenna-in-a-box" geometries fabricated by Punj et al.[5]

**ADVANCED
SCIENCE NEWS**

www.advancedsciencenews.com

**ADVANCED
MATERIALS**

www.advmat.de

Although FIB milling provides sensitive control over the size and shape of the structure with real-time feedback, it is considerably time-consuming, requires substantial optimization, and is not easily automated. The technique is therefore less often used for high volume applications, with the exception of simple designs such as zero-mode waveguides.[87] Instead, it serves as an excellent tool for investigating new plasmonic structures.[16] To date, FIB has been used to fabricate plasmonic nanopore devices on a chip-by-chip basis. In these cases, alignment markers are used to visualize the membrane in the FIB setup, and a sacrificial layer such as silicon dioxide (SiO_2) is used to support the membrane during processing. Raza et al. fabricated double nanohole nanoapertures on 60 nm SiN_x and 500 nm SiO_2 by aligning to four diagonal markers at the corners of the membrane, which were wet-etched into Au and Cr. After removal of the SiO_2 layer, the structure was milled using a neon gas field ion source, which provides the advantage of precision machining with speed.[88] While the authors note complications in using a gallium ion FIB, which is typically used for massive material removal, Crick et al. used gallium ion FIB to mill plasmonic bullseye features into 50 nm gold (Figure 5c). This required sequences of test milling and visual inspection in order to establish the ideal milling conditions, as in some instances overmilling (partial or total removal of the gold), undermilling (undefined features), or membrane perforation occurred.[89] To facilitate drilling of nanopores (20 nm), a helium ion beam was used (Carl Zeiss ORION NanoFab).

2.3. Metallized Nanopores

Localized enhancement can also be achieved by coating a nanopore with metal. In one configuration, Li et al. fabricated 10 nm nanopores by sputtering 10 nm of titanium and 200 nm of gold on a silicon nanocavity.[90,91] Nanopores in free-standing membranes can be coated with metal, provided that the membrane and nanopore can withstand the high temperature of the chosen deposition method. Controlled breakdown (CBD) offers a way to generate nanopores directly in metallized membranes, although the cross-sectional geometry of the resulting pore has yet to be determined.[92–94]

2.4. Drilling Nanopores

To fabricate nanopores, researchers have traditionally relied on focused electron or ion beam methods, namely transmission electron microscopy (TEM) and focused ion beam (FIB) milling.[95–98] However, the high cost and low throughput of these methods has led to the development of several new approaches, which may be beneficial for the fabrication of plasmonic devices. For instance, if FIB is used to fabricate the plasmonic architecture, FIB can also be used to drill the nanopore, after the appropriate adjustments to the ion source. A gallium ion beam, which is typically used to remove massive material in plasmonic devices, can readily drill nanopores with a diameter of several hundred nanometers, but the diameter can be reduced to less than 5 nm by shrinking a large pore with the ion beam.[97,99,100] Additionally, conformal atomic layer deposition

(ALD) processes have been used to shrink FIB-drilled nanopores from roughly 30 nm down to 5 nm.[67] Alternatively, systems such as the Carl Zeiss ORION NanoFab are capable of switching between a gallium and helium ion FIB, allowing the plasmonic layer to be fabricated using the gallium beam, and the nanopore to be formed using the helium beam.[89]

An EBL-based approach was used to fabricate nanopores in a nonplasmonic device, but only for diameters larger than 16 nm (±10%) which precludes their use for some sensing applications.[101] Helium ion milling can be used to make sub-5 nm nanopores with high reproducibility (<10% variability in pore size), but, similarly to high-resolution TEM, remains prohibitively expensive for many laboratories.[72,102,103] The lowest cost alternative, controlled dielectric breakdown (CBD), has been shown to be effective for creating a range of pore sizes in various materials, for ssDNA, dsDNA, and protein sensing.[73,92–94] Although it is an inherently stochastic process, CBD can be automated for fabricating 2-nm nanopores with high yield, as well as for larger nanopores.[104]

CBD has also been used in one of the first demonstrations of an integrated plasmonic nanopore device with a sub-10 nm nanopore (Figure 5b). It was shown that simultaneously applying a transmembrane voltage and illuminating with a 785 nm laser consistently caused a nanopore to form at the center of a bowtie structure.[77] Although elevated temperatures are known to accelerate dielectric breakdown,[105] the temperature profile was found to be nearly uniform around the 100 nm structure, and the localization was instead attributed to the plasmonic optical field enhancement. An alternative self-alignment strategy is to selectively thin the membrane at the desired nanopore location (e.g., by FIB, RIE) prior to CBD, as demonstrated by Carlsen et al. and Zrehen et al. The membrane would thus be biased to form a nanopore within the thinned region.[106,107]

One of the drawbacks of CBD is the careful optimization required to prevent the unintended formation of multiple pores on a single membrane.[107,108] For high-throughput sensing where multiple nanopores are desirable, studies have presented possible ways to determine the number of pores formed.[109,110] However, these pores form at random locations, and their size is not easily controlled since the further application of an electric field to induce dielectric breakdown may expand existing pores. This problem was remedied using microscale liquid contacts for a nanopore pitch of 5 μm,[111] though the controlled formation of nanopore arrays with sub-micrometer pitch has not yet been demonstrated. The ion track-etching (ITE) technique,[112] which is the most efficient at generating nanopores (billions cm^{-2}), is also a fundamentally stochastic process with poor spatial control.
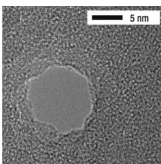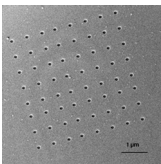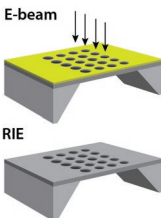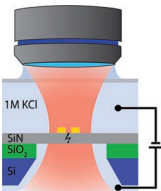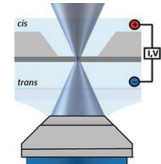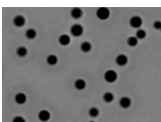
The latest nanopore fabrication method, which is based on laser-induced etching, combines several advantages of CBD (low cost, simplicity) with the well-defined pore localization typically achieved with ion and electron beam techniques. Specifically, this technique uses a milliwatt laser to gradually etch free-standing SiN_x membranes directly in aqueous solution, until a nanopore is formed. As the laser can be positioned anywhere on the membrane, it provides diffraction-limited control of the nanopore position, as well as the possibility to create multiple spatially separated pores.[113] Laser etching can be fine-tuned to form pores consistently with nearly 100% yield. But being an

emerging method, further studies are required to better characterize and improve pore functionality especially below 3 nm, as well as to determine the stability and yield. However, being a new technique, laser etching has not yet been used to fabricate nanopores in plasmonic devices. The ability to do so depends on the interaction of light with the plasmonic structure.

A comparison of the various techniques is summarized in **Table 1**, which includes a column dedicated to whether the technique has been used for a plasmonic device in the past. The choice of nanopore fabrication technique primarily depends on the intended sensing application, as this determines the size of the nanopore. For instance, unzipping of dsDNA requires a pore with a diameter similar to that of ssDNA ($\approx$1.1 nm).[64] For highly localized plasmonic hotspots, methods capable of precisely positioning pores, such as TEM or FIB, are preferred. CBD is an easy-to-implement, low-cost method; however, it is unclear how reproducibly it can fabricate a single nanopore at a specific location. In situ laser etching bears the potential to perform highly localized pore drilling, however, as an emerging method more studies need to be performed. Furthermore, the nature of "self-aligning" nanopores formed within the hotspot of a plasmonic bowtie[77] may not necessarily carry over to other plasmonic designs. While lithography-based nanopore fabrication appears compatible with a wafer-scale EBL process used for the

Table 1. Comparison of nanopore drilling techniques, indicating whether the drilling technique has been specifically used in a plasmonic device. Pore size range is based on literature for nanopore fabrication. *Cost* refers to instrument expense. "Throughput" accounts for average time to form a single pore and scalability of the process. "Alignment" indicates how accurately and easily a nanopore can be positioned at a set location. Attribution of images as follows: TEM: adapted with permission.[98] Copyright 2003, Nature Publishing Group; FIB/HIM: authors' own; EBL/RIE: authors' own; CBD: adapted with permission.[77] Copyright 2015, American Chemical Society; Laser: adapted under the terms of the CC-BY Creative Commons Attribution 4.0 International License (http://creativecommons.org/licenses/by/4.0/).[113] Copyright 2018, The Authors, published by Springer Nature; ITE: adapted with permission.[112] Copyright 2009, National Academy of Sciences.

		Used in plasmonics	Size [nm]	Cost	Throughput	Alignment	Ref.
TEM		✓	<1–20	High	Low	High	[95–98]
FIB/HIM		✓	4–200	High	High	High	[68,74,91,99,102,104,105]
RIE		X	>16	Medium	High	Low	[101]
CBD		✓	<1–50	Low	Medium	Medium	[73,77,92–94,107,110]
LASER		X	<1–5	Low	Medium	Medium	[113]
ITE		X	1–100	High	High	Low	[112]

1900422 (10 of 18)

plasmonics, it would be challenging to optimize the nanopore size and align various device layers with nanoscale resolution.

3. Label-Free Optical Sensing

Plasmon resonance in metal nanostructures depends strongly on the interaction with analytes in the sensing volume.[3,50] While the locally enhanced electric field in plasmonic hotspots may be used to drive the excitation of fluorescent labels, direct sensing of unlabeled analytes is also possible via changes in the resonance frequency of plasmonic hotspots.

3.1. Plasmonic-Nanopore-Enhanced Resonance Shift Assay

Near-field optical effects around sub-wavelength apertures in tapered optical fibers have been used to probe single molecules on surfaces in near-field scanning optical microscopy.[114] This concept has been extended to apertures in thin metal films, forming ZMWs in which analytes are excited within zeptoliter observation volumes.[115] Shi et al. used a ZMW to measure changes in refractive index due to analytes entering the ZMW directly above a nanopore.[99] An analyte entering the sensing volume causes the apparent refractive index of the aperture to increase with respect to its empty configuration. This change in refractive index affects the resonance that excites the gap, leading to an increased transmission of scattered light through the nanopore (**Figure 6**). In addition to improving scattering, the 100 nm thick gold film suppressed the optical background signal by blocking incident light in a dark-field configuration. The large diameter (150–200 nm) of the nanopores fabricated in these devices enabled detection of 70 nm polystyrene beads with an increase in scattering intensity of 20–50%. However, achieving the same level of sensitivity for molecular analytes
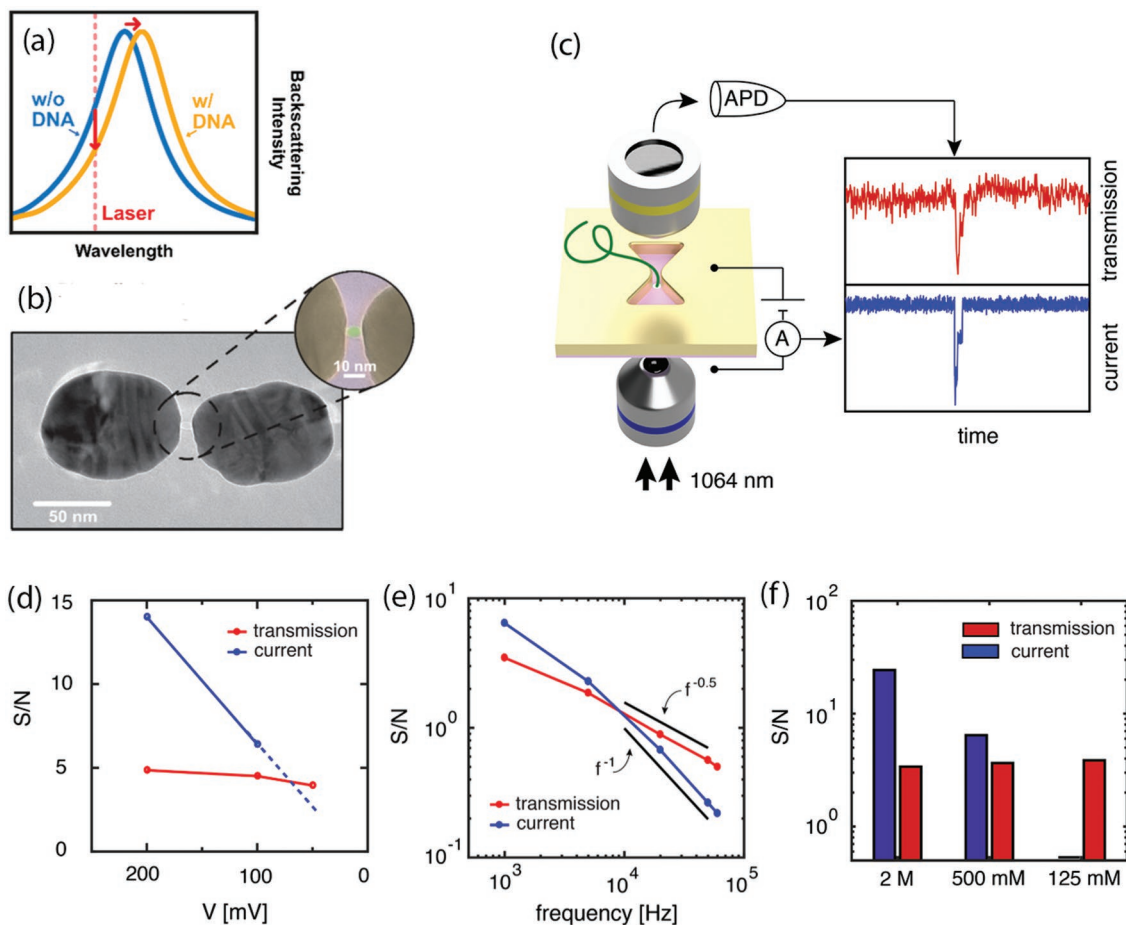
Figure 6. Single-molecule nanopore sensing based on refractive index changes. a) Illustration of the sensing principle. The presence of an analyte increases the refractive index of the sensing volume, leading to a redshifted resonance peak of the plasmonic structure. This can be measured as a decrease in the intensity of backscattered light through a nanopore between a gold nanodisc antenna. Adapted with permission.[116] Copyright 2018, American Chemical Society. b) Typical TEM image of the plasmonic nanopore device from (a). Adapted with permission.[116] Copyright 2018, American Chemical Society. c) The ionic current through the nanopore and the light transmitted through an inverted bowtie nanoantenna show a strong correlation upon translocation of DNA. Adapted with permission.[79] Copyright 2018, American Chemical Society. d–f) Comparison of the signal-to-background ratio (SBR) for optical and ionic current measurements of the device in (c) under various experimental conditions. In contrast to the ionic SBR, the optical SBR is independent of operating voltage and ionic strength, and it enables a higher measurement bandwidth. d–f) Adapted with permission.[79] Copyright 2018, American Chemical Society.

remains challenging due to the much smaller expected index change.

Verschueren et al. applied the concept of resonance sensing to a plasmonic inverted bowtie nanoantenna.[79] The change of intensity of the transmitted light was attributed to a redshifted resonance of the nanoantenna in the presence of analytes (Figure 6b). This hypothesis was confirmed by independent measurements[116] that showed a decrease or increase of the backscattered signal when the excitation wavelength was respectively lower or higher than the resonant wavelength of the nanoantenna. The use of an inverted bowtie antenna enabled detection of folded dsDNA, but the SBR was insufficient for regular detection of linear dsDNA.[79] These results highlighted a strong dependence of the gap resonance on the polarization of the incident light, and excitation was only achieved when the polarization was parallel to the nanogap. A detailed quantification also demonstrated key advantages of optical sensing over ionic sensing (Figure 6c). First, the magnitude of the optical signal is independent of the driving voltage and buffer composition. Second, the optical noise spectrum is constant at high frequencies, enabling measurements at higher bandwidth and a slower deterioration of SBR than for ionic sensing. Nevertheless, achieving high SBR still appears to be a bottleneck for single-molecule plasmonic resonance shift sensing.

3.2. Plasmonic-Nanopore-Enhanced SERS Assay

Although changes in the refractive index within a plasmonic sensor's hotspot offer a simple means to detect analytes without the need for labeling, single-wavelength measurements provide limited information about the analyte, as different molecules may yield similar signals. Limited specificity complicates detection in complex samples containing diverse analytes. Surface-enhanced Raman spectroscopy (SERS) overcomes this challenge by using plasmonic hotspots to excite chemical bonds at their resonant wavelengths, thereby providing rich structural information characteristic to each analyte; however, SERS is limited by the brief residence time of molecules within the hotspot (typically ≈1 μs for free diffusion) in acquiring spectral information (several ms to tens of ms). Moreover, it is challenging to resolve single molecules, as multiple hotspots may be occupied by different analytes at a given time.

Combining nanopores with SERS provides a way to extend the observation time, by sequentially threading molecules through the hotspot. However, typical sub-millisecond translocation times are still too short to acquire the full spectrum multiple times during translocation (a requirement to reliably measure the spectrum of a single translocating molecule). The Van Dorpe group extended the interaction time of analytes with the hotspot by using nanoslit devices to optically trap particles in the plasmonic hotspot (**Figure 7a**).[117,118] Although they demonstrated detection of DNA oligonucleotides[119] and dielectric nanoparticles,[120] the nanoslit devices could not be used to collect ionic signatures of translocating molecules due to the large cross-sectional area of the slit and the metal sidewall of the nanoslit. As such, nanoslit devices were only suitable for *fluidic* nanoslit SERS, and no transmembrane voltage was applied. A notable exception is the work of Chen et al. in which a transmembrane voltage was used to drive adsorption and translocation of analytes.[121] Electrophoretic translocation through a nanopore is particularly useful for large polymer molecules, as it untangles and sequentially exposes different parts of the molecule to the hotspot. However, the high ionic background signal and photoinduced electrical noise[122] in metallic nanopores remains a challenge, and resistive pulse sensing has not yet been shown in nanoslit devices.

Belkin et al. proposed and simulated controlled ratcheting of DNA through a nanopore, by using optical trapping and release of DNA by exciting a bowtie nanoantenna with microsecond pulses (Figure 7b).[123] Simulations showed that combining this process with SERS would enable accurate piecewise sequencing of DNA. However, to resolve the sequence, the tail of incoming DNA must be untangled to prevent accumulation and coiling near the hotspot, and it is not clear how this can be practically implemented.

Experimental demonstrations of SERS with nanopores based on dielectric membranes showed that fluorescently labeled metallic nanoparticles could be detected during translocation.[124] By using a fast acquisition system (less than 1 ms for the measured spectrum) and fluorescently labeled nanoparticles with long translocation times (>50 ms), the Raman spectrum could be measured several times during a single translocation (Figure 7c). The use of nonresonant SERS for unlabeled analytes may suffer from lower SNR and will likely not be possible for molecular analytes with sub-millisecond translocation times, until acquisition times can be further reduced.

Nanopipettes can be used to probe localized targets such as cells, which cannot easily be delivered to conventional nanopores. Plasmonic effects in the vicinity of metal-coated tips have been leveraged in tip-enhanced Raman spectroscopy (TERS),[125] and several examples exist of TERS and SERS sensing using nanopipettes. For instance, Freedman et al. showed label-free sensing using plasmonic nanopipettes, by using a dielectrophoretic assembly of gold colloids to form a rough gold sphere at the tip of a nanopipette.[126] This created multiple plasmonic hotspots, which acted as an SERS substrate at the tip of the nanopipette that could also be used for TERS. Passive self-assembly of gold nanospheres to create SERS tips has also been shown by Liu et al.[127] However, the use of nanopipette-based plasmonic nanopores for SERS faces several challenges. First, the pore size commonly achieved with laser-based pipette pullers (≈50 nm) is too large to identify most molecular analytes. More importantly, the random formation of multiple hotspots complicates the discrimination of single-molecule translocation events and limits repeatability.

The two dominant approaches to label-free sensing using plasmonic nanopores (resonance shift and SERS) are both suitable for single-analyte fingerprinting but differ in the depth of information they provide about an analyte. Although resonance shift sensing is relatively straightforward to implement, it does not provide spectral information and requires a priori knowledge of the sample, as different analytes may yield similar signatures. On the other hand, SERS sensing using nanopores provides very rich information, but long acquisition times limit the use of this technique to large analytes with a lower translocation velocity. Nevertheless, it is easy to imagine that a combination of controlled translocations, enabled by nanopore
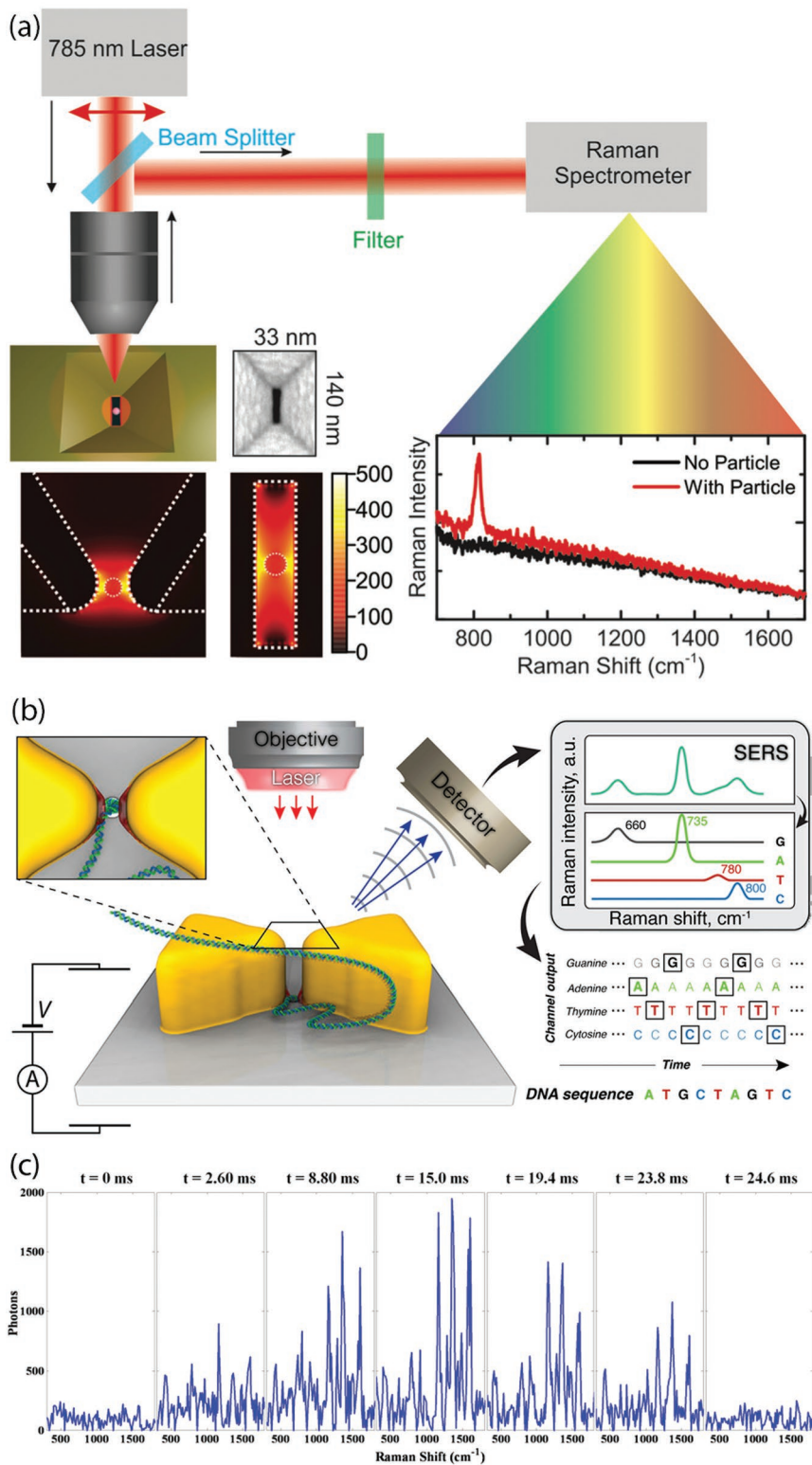
Figure 7. Single-molecule nanopore sensing based on SERS. a) Schematic of SERS detection of dielectric nanoparticles using a gold-coated nanoslit geometry. A nanoparticle is trapped by optical forces in the nanoslit at the bottom of the cavity, enabling long acquisition times. Adapted with permission.[120] Copyright 2015, Royal Society of Chemistry. b) Schematic of DNA threading through a nanopore with a bowtie antenna. The measured spectrum is the superposition of the Raman spectrum of individual nucleobases. Adapted with permission.[123] Copyright 2015, American Chemical Society. c) Sub-millisecond acquisition time for the full Raman spectrum enables multiple acquisitions during a single translocation of a gold nanoparticle. Adapted with permission.[124] Copyright 2013, American Chemical Society.

**ADVANCED
SCIENCE NEWS**
www.advancedsciencenews.com

**ADVANCED
MATERIALS**
www.advmat.de

threading, and fast spectrometers can make this approach relevant to fingerprinting of molecular analytes, and possibly even of long polymers.

4. Plasmonic-Nanopore-Enhanced Fluorescence Sensing

Among all single-molecule sensing methods, fluorescence provides one of the highest signal-to-background time-resolved signals.[128] A bright fluorophore typically has a large absorption cross-section ($\approx 10^5$ mol^{-1} cm^{-1}) and can emit thousands of photons in a millisecond, enabling time-resolved single-molecule sensing with low background. Additionally, labeling of nucleic acids and proteins is an established area, and stable fluorophores are widely available, covering wavelengths from the near UV to the near IR. Consequently, single-molecule fluorescence

sensing involving spectral multiplexing has become feasible, supporting biomedical applications such as DNA sequencing.

One of the challenges of coupling nanopores with single-molecule fluorescence is related to the fast translocation of molecules through the nanopore, which practically limits the observation time of each fluorophore. Incorporating a plasmonic hotspot in the vicinity of the nanopore may alleviate this challenge. Plasmon-enhanced fluorescence detection has been demonstrated for analytes passing through a hotspot integrated with "nano-holes" on the order of 100 nm wide.[87,129–131] Nanoholes are commonly used due to the challenge of fabricating small nanopores (<10 nm) within multilayer, multimaterial devices. However, they are unsuitable for resistive pulse sensing and translocation of one molecule at a time, as their diameter is much larger than most biological analytes. Recently, Assad et al. reported a device, with a nanopore positioned within a plasmonic nanowell (**Figure 8**a). A 4 nm diameter pore was formed
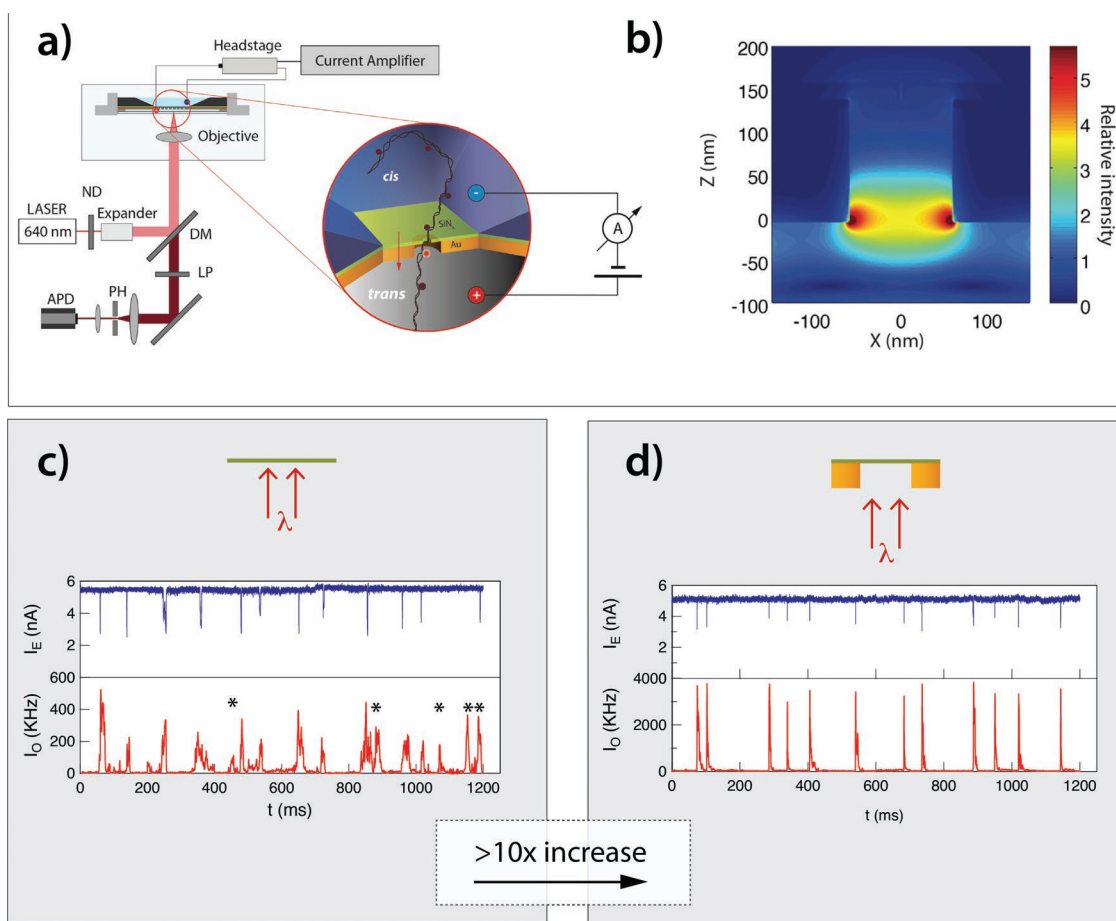
Figure 8. Simultaneous electrical and optical recording of DNA translocations through solid-state nanopores. a) A simplified illustration of the electro-optical nanopore setup. A collimated laser beam is focused at the nanopore region through the microscope objective lens, forming a tight focus spot for confocal illumination. The emitted photons are directed to an avalanche photodiode. Inset: a schematic cross-section of the PNW–NP device containing a nanowell fabricated in a gold film (orange) with a nanopore drilled in the freestanding SiN$_x$ membrane (light green). b) FDTD simulation 2D heat map of the excitation intensity at 680 nm, calculated for a 120 nm PNW–NP device. Scale is relative to the STD device. c,d) Representative electro-optical traces of DNA translocation events recorded using two device configurations: "STD" and "PNW–NP." Each panel presents typical concatenated traces of 5 kbp DNA covalently labeled with seven CF640R dyes. Electrical ion current shown in blue and optical signals in red. Asterisks correspond to photon spikes that are not associated with DNA translocations, observed only in the STD device. The optical translocation signal recorded using the plasmonic nanowell–nanopore configuration is enhanced by a factor of 10 as compared to the standard nanochip device configuration. a–d) Adapted with permission.[76] Copyright 2017, Wiley-VCH.

ADVANCED
SCIENCE NEWS
www.advancedsciencenews.com

ADVANCED
MATERIALS
www.advmat.de

at the bottom of a 120 nm wide, 130 nm deep gold nanowell, as described in Section 2.1. The dimensions of the plasmonic nanowell were chosen based on numerical simulation, to provide peak plasmon-induced fluorescence enhancement at the epi-illuminated aperture, and to reduce excitation along the optical axis in order to suppress background from analytes in the *cis* reservoir (Figure 8a). An intensity heatmap of the plasmonic nanowell–nanopore (PNW–NP) cross-section is shown in Figure 8b.

In addition to its geometry, the orientation of the device with respect to incoming light had an important impact on sensor performance. The device was examined in two orientations: a ZMW configuration, in which the laser excitation was introduced from the SiN_x membrane side, and a PNW configuration, in which the laser excitation was introduced from the plasmonic (nanowell) side. In both cases, the emission light was collected in epi-fluorescence mode. Fluorophore solutions of various concentrations were introduced at the side opposite of the excitation, and the background fluorescence was measured. The background threshold for Cy5 dyes introduced at the nanowell side was 0.1×10^{-9} M, whereas the background was essentially negligible up to 1×10^{-3} M in the PNW configuration. The difference in the background levels was due to the fact that the SiN_x membrane blocks free molecules from entering the PNW. Only a single molecule can enter the nanopore at a time, thus reducing the apparent background level.

To characterize the properties of PNW–NP, 5 kbp dsDNA was covalently labeled with the fluorophore CF640R. Each DNA molecule harbored 7 fluorophores and was introduced to the *cis* chamber at relatively low concentrations of 0.1×10^{-9} M or less (Figure 8a). Relative to a nonplasmonic device, the PNW exhibited more than tenfold increase in peak fluorescence intensity during the passage of the DNA molecules (Figure 8c,d). Additionally, the inclusion of the PNW–NP completely suppressed spurious photon spikes from collisional events and allowed sub-millisecond synchronization between the electrical and optical signals. These results demonstrate both fluorescence enhancement from the plasmonic layer, as well as the use of resistive pulse sensing as a "gating" signal. A detailed analysis of the translocation results yielded a per-fluorophore SBR of 33 in the PNW configuration, versus less than 3 for a standard (STD) SiN membrane containing a nanopore, which was consistent for both low and high excitation powers (9 and 90 μW).

The PNW–NP example shows that the combination of plasmonics and nanopores is very powerful, providing i) serial, linearized interrogation, particularly for enhanced specificity via optically barcoded analytes; ii) fluorescent signal enhancement from the plasmonic layer; and iii) a superior capture rate relative to typical ZMWs lacking active focusing, made possible by the nanopore. Notably, a ZMW used in conjunction with a nanopore may offer enhanced detection rates under an applied nanopore bias, independently of plasmon resonance.[132]

5. Additional Plasmon-Induced Effects in Nanopores

The temperature of the solution in the vicinity of a nanopore directly and indirectly affects its performances. The mobility of ions and the interactions of analytes with the pore are strongly temperature-dependent.[60,63] Changes to the temperature will impact the nanopore conductance (*G*), blockage amplitude (Δ*G*), translocation dwell time (τ), and capture rate.[133,134] Around room temperature the pore conductance increases roughly linearly with temperature (d*G*/d*T* = 0.21 nS K⁻¹), and a change of 35 °K results in a doubling of the pore conductance and blockage amplitude. While the latter is desirable for improved signal-to-noise, a raised temperature also speeds up translocation, thereby lower the sensing resolution. In an experiment with ≈50 kbp long lambda phage DNA, the translocation dwell time across an 8.1 nm pore decreased from ≈2.1 ms at 285 °K to ≈0.9 ms at 318 °K after heating the whole flow cell with a Peltier element.[134] For the same experimental conditions, the capture rate was observed to approximately double over the same temperature range. This was due to an increase in the electrophoretic mobility of the biomolecule, which varies according to the balance between electric pull and viscous drag, which at high concentrations can be expressed as $\mu \propto r_D/\eta$, where r_D is the Debye screening length and η is the viscosity.[135]

In the first application of a nanopore as a temperature probe, it was found that a strong infrared laser (1064 nm, 960 mW) focused directly on a nanopore could raise the local temperature by up to 20 °C, as determined from the change in open pore conductance.[136] Since then, researchers have attempted to exploit the light-concentrating properties of plasmonic nanostructures to increase the heat generation efficiency and localization in nanopore devices.[137] To map optical intensity landscapes of low intensity lasers, Jonsson et al. constructed a gold plasmonic bowtie structure with a nanopore at its center, and as a proof of concept, illuminated it with a near-IR 785 nm 10 mW laser while measuring the ionic conductance. Due to the very strong light absorption of the plasmonic nanoantenna, reflected as a local temperature increase of 55 °C, the signals were almost two orders of magnitude higher compared to a nanopore without a plasmonic nanoantenna. A similar enhancement was made possible with an optimized gold bullseye structure irradiated at wavelengths in the 500–700 nm range.[89]

While plasmonic nanopores have been successfully applied to tomography and temperature control, with other potential applications such as improving solubility and probing conformational stability,[138] there may be some unwanted side effects of nanopore heating for translocation experiments. For example, irradiation of a plasmonic bowtie with a 532 nm 5 mW laser caused the immediate onset of periodic noise, raising the nanopore noise from ≈25 to ≈160 pA (at 300 mV). At a similar power and higher wavelengths (632, 685 nm), there was no significant change in noise levels.[89] Given that for similar temperature increases (attained at different laser powers), the noise levels were completely different, plasmonic-induced heating should not be considered the origin of the noise; rather the noise is due to the interaction of light with a particular structure. This conclusion was also reached for a gold-coated silicon nanopore, illuminated at 633 and 785 nm, for which the source of the noise was suspected to be plasmon induced electrochemical catalysis.[139]

Concerning the translocation kinetics, Nicoli et al. demonstrated the unintuitive result that while plasmonic heating

**ADVANCED
SCIENCE NEWS**
www.advancedsciencenews.com

**ADVANCED
MATERIALS**
www.advmat.de

increases the capture rate, it comes at no expense to the translocation dwell time.[134,140] This in accordance with a study by Di Fiori et al., which showed that low-intensity green laser light focused on a SiN$_x$ nanopore induces a negative surface charge density, thereby creating an electroosmotic flow in the opposite direction of analytes translocation and leading to the desirable result of slower speeds.[141] The capture rate enhancement was described as a thermophoresis effect, whereby molecules move along thermal gradients,[142] as it was stronger than expected for uniform heating in LiCl. In particular, local heating combined with a negative Soret coefficient (defined as the ratio of the thermal and normal diffusion coefficients), results in a longer capture distance than electrophoresis alone. Thermophoresis depends not only on temperature but also on the size and charge of the molecule, type of salt, and ionic strength, therefore plasmonic nanopore systems need to consider both the analyte and buffer properties in order to maximize the capture rate. The approximately tenfold enhancement achieved here using just a few milliwatts of laser power is a testament to how plasmonics can serve to overcome some of the major bottlenecks of nanopore sensing. It is important to keep in mind that high temperatures (e.g., 50°C) are sufficient to facilitate nucleation of surface bubbles,[143] which for particular geometries can get lodged at the nanopore entrance. These bubbles can disrupt translocation or can be exploited for the purpose of a nanopore switch.[144]

6. Outlook and Summary

The plasmonic-nanopore devices described here combine the exceptional field localization and enhancement of surface plasmonics with the active funneling, location-specific threading, and serial processivity of molecular-scale nanopores for superior single-molecule sensing. The hybridization of plasmonic and nanopore device "layers" improves the dwell time by constricting analytes, and improves the detection rate by enhancing the analyte capture rate through a combination of thermo- and electrophoresis. Initial implementations of this concept that used a simple nanowell–nanopore structure already yielded an order of magnitude fluorescence enhancement in true single molecule sensing.[76] Clearly, however, greater enhancement factors are possible, as well as multiplexed and multimodal analyses with higher spatiotemporal and spectral resolution.

It has already been shown that leveraging the breadth of solid-state fabrication methods enables a variety of PNP implementations. Advances in fabrication will enable novel approaches for designing, applying, and scaling PNP sensors. For example, it is well established that lattices of nanostructures, such as "well"-like apertures, generate significant intra-well resonances that can further enhance inter-well plasmon intensity.[37] Although PNW–NPs have thus far been implemented as stand-alone devices, robust fabrication of arrays would potentially lead to significant gains in SBR, sample volume processivity and detection rate.

Nanopore-assisted threading through a plasmonic hotspot offers an interesting route toward a range of fingerprinting and sequencing applications, particularly for SERS, whose label-free detection bypasses challenges with multiplexing that other optical methods may face. Some applications include high-sensitivity genotyping based on extremely small DNA copy numbers, DNA sequencing, and quantification of epigenetic markers. Finally, although this progress report focused on the development of solid-state plasmonic nanopores, transposing these principles to the expanding field of self-assembled DNA origami structures is only a matter of time, as plasmonic resonators[145] and nanometric apertures[146] have already been demonstrated in this context.

Conflict of Interest

The authors declare no conflict of interest.

[1] X. S. Xie, *JAMA, J. Am. Med. Assoc.* **2015**, *313*, 2021.
[2] S. O. Kelley, *ACS Sens.* **2017**, *2*, 193.
[3] A. B. Taylor, P. Zijlstra, *ACS Sens.* **2017**, *2*, 1103.
[4] E. Di Fabrizio, S. Schlücker, J. Wenger, R. Regmi, H. Rigneault, G. Calafiore, M. West, S. Cabrini, M. Fleischer, N. F. van Hulst, M. F. Garcia-Parajo, A. Pucci, D. Cojoc, C. A. E. Hauser, M. Ni, *J. Opt.* **2016**, *18*, 063003.
[5] D. Punj, M. Mivelle, S. B. Moparthi, T. S. van Zanten, H. Rigneault, N. F. van Hulst, M. F. García-Parajó, J. Wenger, *Nat. Nanotechnol.* **2013**, *8*, 512.
[6] D. Darvill, A. Centeno, F. Xie, *Phys. Chem. Chem. Phys.* **2013**, *15*, 15709.
[7] M. I. Stockman, K. Kneipp, S. I. Bozhevolnyi, S. Saha, A. Dutta, J. Ndukaife, N. Kinsey, H. Reddy, U. Guler, V. M. Shalaev, A. Boltasseva, B. Gholipour, H. N. S. Krishnamoorthy, K. F. Macdonald, C. Soci, N. I. Zheludev, V. Savinov, R. Singh, P. Gro, C. Lienau, M. Vadai, M. L. Solomon, D. R. Barton, M. Lawrence, J. A. Dionne, *J. Opt.* **2018**, *20*, 043001.
[8] A. Kinkhabwala, Z. Yu, S. Fan, Y. Avlasevich, K. Müllen, W. E. Moerner, *Nat. Photonics* **2009**, *3*, 654.
[9] P. Zijlstra, P. M. R. Paulo, M. Orrit, *Nat. Nanotechnol.* **2012**, *7*, 379.
[10] K. M. Mayer, F. Hao, S. Lee, P. Nordlander, J. H. Hafner, *Nanotechnology* **2010**, *21*, 255503.
[11] D. W. Deamer, M. Akeson, D. Branton, *Nat. Biotechnol.* **2016**, *34*, 518.
[12] B. N. Miles, A. P. Ivanov, K. A. Wilson, F. Doğan, D. Japrung, J. B. Edel, *Chem. Soc. Rev.* **2013**, *42*, 15.
[13] L. Novotny, N. F. van Hulst, *Nat. Photonics* **2011**, *5*, 83.
[14] L. Novotny, B. Hecht, in *PrincIples of Nano-Optics*, Cambridge University Press, Cambridge, UK **2014**, pp. 369–413.

[15] A. Portela, T. Yano, C. Santschi, H. Matsui, T. Hayashi, M. Hara, O. J. F. Martin, H. Tabata, *Appl. Phys. Lett.* **2014**, *105*, 091105.

[16] M. Jahn, S. Patze, I. J. Hidi, R. Knipper, A. I. Radu, A. Mühlig, S. Yüksel, V. Peksa, K. Weber, T. Mayerhöfer, D. Cialla-May, J. Popp, *Analyst* **2016**, *141*, 756.

[17] A. E. Cetin, S. Aksu, M. Turkmen, D. Etezadi, H. Altug, *J. Electromagn. Waves Appl.* **2015**, *29*, 1686.

[18] K. Kneipp, H. Kneipp, V. Kartha, R. Manoharan, G. Deinum, I. Itzkan, R. R. Dasari, M. Feld, *Physical Review E* **1998**, *57*, R6281.

[19] S. V Boriskina, J. K. Tong, W. C. Hsu, B. Liao, Y. Huang, V. Chiloyan, G. Chen, *Nanophotonics* **2016**, *5*, 134.

[20] C. Dekker, *Nat. Nanotechnol.* **2007**, *2*, 209.

[21] M. Wanunu, W. Morrison, Y. Rabin, A. Y. Grosberg, A. Meller, *Nat. Nanotechnol.* **2010**, *5*, 160.

[22] T. Gilboa, A. Meller, *Analyst* **2015**, *140*, 4733.

[23] S. W. Kowalczyk, A. Y. Grosberg, Y. Rabin, C. Dekker, *Nanotechnology* **2011**, *22*, 315101.

[24] A. H. Squires, E. Atas, A. Meller, *PLoS One* **2015**, *10*, e0142944.

[25] E. C. Yusko, B. R. Bruhn, O. M. Eggenberger, J. Houghtaling, R. C. Rollings, N. C. Walsh, S. Nandivada, M. Pindrus, A. R. Hall, D. Sept, J. Li, D. S. Kalonia, M. Mayer, *Nat. Nanotechnol.* **2017**, *12*, 360.

[26] J. Clarke, H. C. Wu, L. Jayasinghe, A. Patel, S. Reid, H. Bayley, *Nat. Nanotechnol.* **2009**, *4*, 265.

[27] N. A. W. Bell, U. F. Keyser, *Nat. Nanotechnol.* **2016**, *11*, 645.

[28] K. Chen, J. Kong, J. Zhu, N. Ermann, P. Predki, U. F. Keyser, *Nano Lett.* **2019**, *19*, 1210.

[29] B. McNally, A. Singer, Z. Yu, Y. Sun, Z. Weng, A. Meller, *Nano Lett.* **2010**, *10*, 2237.

[30] J. B. Khurgin, *Nat. Nanotechnol.* **2015**, *10*, 2.

[31] P. R. West, S. Ishii, G. V Naik, N. K. Emani, V. M. Shalaev, A. Boltasseva, *Laser Photonics Rev.* **2010**, *4*, 795.

[32] G. V. Naik, V. M. Shalaev, A. Boltasseva, *Adv. Mater.* **2013**, *25*, 3264.

[33] D. K. Gramotnev, S. I. Bozhevolnyi, *Nat. Photonics* **2010**, *4*, 83.

[34] N. Liu, T. Liedl, *Chem. Rev.* **2018**, *118*, 3032.

[35] A. Gopinath, S. V Boriskina, N. N. Feng, B. M. Reinhard, L. Dal Negro, *Nano Lett.* **2008**, *8*, 2423.

[36] Y. Hong, Y. Qiu, T. Chen, B. M. Reinhard, *Adv. Funct. Mater.* **2014**, *24*, 739.

[37] F. J. Garcia-Vidal, L. Martin-Moreno, T. W. Ebbesen, L. Kuipers, *Rev. Mod. Phys.* **2010**, *82*, 729.

[38] M. Kraft, Y. Luo, S. A. Maier, J. B. Pendry, *Phys. Rev. X* **2015**, *5*, 031029.

[39] I. Malkiel, M. Mrejen, A. Nagler, U. Arieli, L. Wolf, H. Suchowski, *Light: Sci. Appl.* **2018**, *7*, 60.

[40] C. Forestiere, A. J. Pasquale, A. Capretti, G. Miano, A. Tamburrino, S. Y. Lee, B. M. Reinhard, L. Dal Negro, *Nano Lett.* **2012**, *12*, 2037.

[41] T. Feichtner, O. Selig, M. Kiunke, B. Hecht, *Phys. Rev. Lett.* **2012**, *109*, 127701.

[42] G. W. Bryant, F. J. García De Abajo, J. Aizpurua, *Nano Lett.* **2008**, *8*, 631.

[43] I. C. Huang, J. Holzgrafe, R. A. Jensen, J. T. Choy, M. G. Bawendi, M. Lončar, *Appl. Phys. Lett.* **2016**, *109*, 133105.

[44] W. Zhu, R. Esteban, A. G. Borisov, J. J. Baumberg, P. Nordlander, H. J. Lezec, J. Aizpurua, K. B. Crozier, *Nat. Commun.* **2016**, *7*, 11495.

[45] J. B. Khurgin, W. Tsai, D. P. Tsai, G. Sun, *ACS Photonics* **2017**, *4*, 2871.

[46] H. Zhao, P. H. Brown, P. Schuck, *Biophys. J.* **2011**, *100*, 2309.

[47] J. N. Anker, W. P. Hall, O. Lyandres, N. C. Shah, J. Zhao, R. P. Van Duyne, *Nat. Mater.* **2008**, *7*, 442.

[48] S. Chen, M. Svedendahl, R. P. Van Duyne, M. Käll, *Nano Lett.* **2011**, *11*, 1826.

[49] V. Claudio, A. B. Dahlin, T. J. Antosiewicz, *J. Phys. Chem. C* **2014**, *118*, 6980.

[50] M. A. Beuwer, B. Van Hoof, P. Zijlstra, *J. Phys. Chem. C* **2018**, *122*, 4615.

[51] K. Kneipp, H. Kneipp, I. Itzkan, R. R. Dasari, M. S. Feld, *J. Phys.: Condens. Matter* **2002**, *14*, R597.

[52] P. Bharadwaj, L. Novotny, *Opt. Express* **2007**, *15*, 14266.

[53] P. Anger, P. Bharadwaj, L. Novotny, *Phys. Rev. Lett.* **2006**, *96*, 3.

[54] A. Puchkova, C. Vietz, E. Pibiri, B. Wünsch, M. Sanz Paz, G. P. Acuna, P. Tinnefeld, *Nano Lett.* **2015**, *15*, 8354.

[55] D. Branton, D. W. Deamer, A. Marziali, H. Bayley, S. A. Benner, T. Butler, M. Di Ventra, S. Garaj, A. Hibbs, X. Huang, S. B. Jovanovich, P. S. Krstic, S. Lindsay, X. S. Ling, C. H. Mastrangelo, A. Meller, J. S. Oliver, Y. V Pershin, J. M. Ramsey, R. Riehn, G. V Soni, V. Tabard-Cossa, M. Wanunu, M. Wiggin, J. A. Schloss, *Nat. Biotechnol.* **2008**, *26*, 1146.

[56] N. Varongchayakul, D. Huttner, M. W. Grinstaff, A. Meller, *Sci. Rep.* **2018**, *8*, 1017.

[57] M. Wanunu, T. Dadosh, V. Ray, J. Jin, L. McReynolds, M. Drndic, *Nat. Nanotechnol.* **2010**, *5*, 807.

[58] J. J. Kasianowicz, E. Brandin, D. Branton, D. W. Deamer, *Proc. Natl. Acad. Sci. USA* **1996**, *93*, 13770.

[59] M. Akeson, D. Branton, J. J. Kasianowicz, E. Brandin, D. W. Deamer, *Biophys. J.* **1999**, *77*, 3227.

[60] A. Meller, L. Nivon, E. Brandin, J. Golovchenko, D. Branton, *Proc. Natl. Acad. Sci. USA* **2000**, *97*, 1079.

[61] H. Bayley, *Clin. Chem.* **2015**, *61*, 25.

[62] A. Singer, S. Rapireddy, D. H. Ly, A. Meller, *Nano Lett.* **2012**, *12*, 1722.

[63] M. Wanunu, J. Sutin, B. McNally, A. Chow, A. Meller, *Biophys. J.* **2008**, *95*, 4716.

[64] O. N. Assad, N. Di Fiori, A. H. Squires, A. Meller, *Nano Lett.* **2015**, *15*, 745.

[65] R. M. M. Smeets, N. H. Dekker, C. Dekker, *Nanotechnology* **2009**, *20*, 095501.

[66] R. M. M. Smeets, U. F. Keyser, N. H. Dekker, C. Dekker, *Proc. Natl. Acad. Sci. USA* **2008**, *105*, 417.

[67] R. dela Torre, J. Larkin, A. Singer, A. Meller, *Nanotechnology* **2012**, *23*, 385308.

[68] B. N. Anderson, O. N. Assad, T. Gilboa, A. H. Squires, D. Bar, A. Meller, *ACS Nano* **2014**, *8*, 11836.

[69] A. Ivankin, R. Y. Henley, J. Larkin, S. Carson, M. L. Toscano, *ACS Nano* **2014**, *8*, 10774.

[70] H. Yamazaki, S. Kimura, M. Tsukahara, K. Esashika, T. Saiki, *Appl. Phys. A* **2014**, *115*, 53.

[71] T. Gilboa, C. Torfstein, M. Juhasz, A. Grunwald, Y. Ebenstein, E. Weinhold, A. Meller, *ACS Nano* **2016**, *10*, 8861.

[72] F. Sawafta, B. Clancy, A. T. Carlsen, M. Huber, A. R. Hall, *Nanoscale* **2014**, *6*, 6991.

[73] R. Wang, T. Gilboa, J. Song, D. Huttner, M. W. Grinstaff, A. Meller, *ACS Nano* **2018**, *12*, 11648.

[74] P. Rai-Choudhury, *Handbook of Microlithography, Micromachining, and Microfabrication: Microlithography*, SPIE Optical Engineering Press, Bellingham, WA, USA **1997**.

[75] V. R. Manfrinato, L. Zhang, D. Su, H. Duan, R. G. Hobbs, E. A. Stach, K. K. Berggren, *Nano Lett.* **2013**, *13*, 1555.

[76] O. N. Assad, T. Gilboa, J. Spitzberg, M. Juhasz, E. Weinhold, A. Meller, *Adv. Mater.* **2017**, *29*, 1605442.

[77] S. Pud, D. V. Verschueren, N. Vukovic, C. Plesa, M. P. Jonsson, C. Dekker, *Nano Lett.* **2015**, *15*, 7112.

[78] X. Shi, D. V. Verschueren, S. Pud, C. Dekker, *Small* **2018**, *14*, 1703307.

[79] D. V. Verschueren, S. Pud, X. Shi, L. De Angelis, L. Kuipers, C. Dekker, *ACS Nano* **2019**, *13*, 61.

[80] W. Yue, Z. Wang, Y. Yang, L. Chen, A. Syed, K. Wong, X. Wang, *J. Micromech. Microeng.* **2012**, *22*, 125007.

[81] D. Cialla, J. Petschulat, U. Hübner, H. Schneidewind, M. Zeisberger, R. Mattheis, T. Pertsch, M. Schmitt, R. Möller, J. Popp, *Chem Phys Chem* **2010**, *11*, 1918.

[82] Y. Chen, *Microelectron. Eng.* **2015**, *135*, 57.

[83] E. Plum, V. A. Fedotov, A. S. Schwanecke, N. I. Zheludev, Y. Chen, *Appl. Phys. Lett.* **2007**, *90*, 223113.

[84] Y. Chen, K. Peng, Z. Cui, *Microelectron. Eng.* **2004**, *73–74*, 662.

[85] Y. C. Stephen, P. Krauss, P. Renstrom, *J. Vac. Sci. Technol., B: Microelectron. Nanometer Struct.–Process., Meas., Phenom.* **1996**, *14*, 4129.

[86] J. Gierak, D. Mailly, P. Hawkes, R. Jede, L. Bruchhaus, L. Bardotti, B. Frével, P. Mélinon, A. Perez, R. Hyndman, J. P. Jamet, J. Ferré, A. Mougin, C. Chappert, V. Mathet, P. Warin, J. Chapman, *Appl. Phys. A* **2005**, *80*, 187.

[87] T. Auger, E. Bourhis, J. Donnez, A. Durnez, J. M. Di Meglio, L. Auvray, F. Montel, J. Yates, J. Gierak, *Microelectron. Eng.* **2018**, *187–188*, 90.

[88] M. U. Raza, S. S. S. Peri, L.-C. Ma, S. M. Iqbal, G. Alexandrakis, *Nanotechnology* **2018**, *29*, 435501.

[89] C. R. Crick, P. Albella, H. J. Kim, A. P. Ivanov, K. B. Kim, S. A. Maier, J. B. Edel, *ACS Photonics* **2017**, *4*, 2835.

[90] Y. Li, C. Chen, K. Willems, S. Kerman, L. Lagae, G. Groeseneken, T. Stakenborg, P. Van Dorpe, *Adv. Opt. Mater.* **2017**, *5*, 6.

[91] K. Malachowski, R. Verbeeck, T. Dupont, C. Chen, Y. Li, S. Musa, T. Stakenborg, D. Sabuncuoglu Tezcan, P. Van Dorpe, *ECS Trans.* **2013**, *50*, 413.

[92] H. Kwok, K. Briggs, V. Tabard-Cossa, *PLoS One* **2014**, *9*, e92880.

[93] I. Yanagi, R. Akahori, T. Hatano, K. Takeda, *Sci. Rep.* **2015**, *4*, 5000.

[94] H. Kwok, M. Waugh, J. A. Bustamante, K. Briggs, V. Tabard-Cossa, *Adv. Funct. Mater.* **2014**, *24*, 7745.

[95] M. J. Kim, M. Wanunu, D. C. Bell, A. Meller, *Adv. Mater.* **2006**, *18*, 3149.

[96] M. J. Kim, B. McNally, K. Murata, A. Meller, *Nanotechnology* **2007**, *18*, 6.

[97] C. J. Lo, T. Aref, A. Bezryadin, *Nanotechnology* **2006**, *17*, 3264.

[98] A. J. Storm, J. H. Chen, X. S. Ling, H. W. Zandbergen, C. Dekker, *Nat. Mater.* **2003**, *2*, 537.

[99] X. Shi, R. Gao, Y. L. Ying, W. Si, Y. F. Chen, Y. T. Long, *ACS Sens.* **2016**, *1*, 1086.

[100] N. C. Lindquist, A. Lesuffleur, S.-H. Oh, N. J. Wittenberg, H. Im, *Chem. Sci.* **2010**, *1*, 688.

[101] D. V. Verschueren, W. Yang, C. Dekker, *Nanotechnology* **2018**, *29*, 145302.

[102] D. Xia, C. Huynh, S. McVey, A. Kobler, L. Stern, Z. Yuan, X. S. Ling, *Nanoscale* **2018**, *10*, 5198.

[103] J. Yang, D. C. Ferranti, L. A. Stern, C. A. Sanford, J. Huang, Z. Ren, L. C. Qin, A. R. Hall, *Nanotechnology* **2011**, *22*, 285310.

[104] K. Briggs, H. Kwok, V. Tabard-Cossa, *Small* **2014**, *10*, 2077.

[105] M. Kimura, *IEEE Trans. Electron Devices* **1999**, *46*, 220.

[106] A. T. Carlsen, K. Briggs, A. R. Hall, V. Tabard-Cossa, *Nanotechnology* **2017**, *28*, 085304.

[107] A. Zrehen, T. Gilboa, A. Meller, *Nanoscale* **2017**, *9*, 16437.

[108] I. Yanagi, H. Hamamura, R. Akahori, K. Takeda, *Sci. Rep.* **2018**, *8*, 10129.

[109] Y. Wang, C. Ying, W. Zhou, L. de Vreede, Z. Liu, J. Tian, *Sci. Rep.* **2018**, *8*, 1234.

[110] C. Ying, J. Houghtaling, O. M. Eggenberger, A. Guha, P. Nirmalraj, S. Awasthi, J. Tian, M. Mayer, *ACS Nano* **2018**, *12*, 11458.

[111] C. E. Arcadia, C. C. Reyes, J. K. Rosenstein, *ACS Nano* **2017**, *11*, 4907.

[112] I. Vlassiouk, P. Y. Apel, S. N. Dmitriev, K. Healy, Z. S. Siwy, *Proc. Natl. Acad. Sci. USA* **2009**, *106*, 21039.

[113] T. Gilboa, A. Zrehen, A. Girsault, A. Meller, *Sci. Rep.* **2018**, *8*, 9765.

[114] E. Betzig, J. K. Trautman, *Science* **1992**, *257*, 189.

[115] M. J. Levene, J. Korlach, S. W. Turner, M. Foquet, H. G. Craighead, W. W. Webb, *Science* **2003**, *299*, 682.

[116] X. Shi, D. V. Verschueren, C. Dekker, *Nano Lett.* **2018**, *18*, 8003.

[117] C. Chen, J. A. Hutchison, P. Van Dorpe, R. Kox, I. De Vlaminck, H. Uji-I, J. Hofkens, L. Lagae, G. Maes, G. Borghs, *Small* **2009**, *5*, 2876.

[118] C. Chen, J. A. Hutchison, F. Clemente, R. Kox, H. Uji-I, J. Hofkens, L. Lagae, G. Maes, G. Borghs, P. Van Dorpe, *Angew. Chem., Int. Ed.* **2009**, *48*, 9932.

[119] C. Chen, J. Ye, Y. Li, L. Lagae, T. Stakenborg, P. Van Dorpe, *IEEE J. Sel. Top. Quantum Electron.* **2013**, *19*, 4600707.

[120] S. Kerman, C. Chen, Y. Li, W. Van Roy, L. Lagae, P. Van Dorpe, *Nanoscale* **2015**, *7*, 18612.

[121] C. Chen, Y. Li, S. Kerman, P. Neutens, K. Willems, S. Cornelissen, L. Lagae, T. Stakenborg, P. Van Dorpe, *Nat. Commun.* **2018**, *9*, 1733.

[122] Y. Li, C. Chen, K. Willems, L. Lagae, G. Groeseneken, T. Stakenborg, P. Van Dorpe, *Nanoscale* **2016**, *8*, 12324.

[123] M. Belkin, S. Chao, M. P. Jonsson, C. Dekker, A. Aksimentiev, *ACS Nano* **2015**, *9*, 10598.

[124] M. P. Cecchini, A. Wiener, V. A. Turek, H. Chon, S. Lee, A. P. Ivanov, D. W. Mccomb, J. Choo, T. Albrecht, S. A. Maier, J. B. Edel, *Nano Lett.* **2013**, *13*, 4602.

[125] R. M. Stöckle, Y. D. Suh, V. Deckert, R. Zenobi, *Chem. Phys. Lett.* **2000**, *318*, 131.

[126] K. J. Freedman, C. R. Crick, P. Albella, A. Barik, A. P. Ivanov, S. A. Maier, S. H. Oh, J. B. Edel, *ACS Photonics* **2016**, *3*, 1036.

[127] H. L. Liu, J. Cao, S. Hanif, C. Yuan, J. Pang, R. Levicky, X. H. Xia, K. Wang, *Anal. Chem.* **2017**, *89*, 10407.

[128] P. R. Selvin, T. Ha, *Single Molecule Techniques A Laboratory Manual*, Cold Spring Harbor Laboratory Press, Cold Spring Harbor, NY, USA **2008**.

[129] X. Li, M. Soler, C. Szydzik, K. Khoshmanesh, J. Schmidt, G. Coukos, A. Mitchell, H. Altug, *Small* **2018**, *14*, 1800698.

[130] C. Escobedo, A. G. Brolo, R. Gordon, D. Sinton, *Nano Lett.* **2012**, *12*, 1592.

[131] T. Ohno, C. Wadell, S. Inagaki, J. Shi, Y. Nakamura, S. Matsushita, T. Sannomiya, *Opt. Mater. Express* **2016**, *6*, 1594.

[132] J. Larkin, M. Foquet, S. W. Turner, J. Korlach, M. Wanunu, *Nano Lett.* **2014**, *14*, 6023.

[133] A. Meller, D. Branton, *Electrophoresis* **2002**, *23*, 2583.

[134] D. V. Verschueren, M. P. Jonsson, C. Dekker, *Nanotechnology* **2015**, *26*, 234004.

[135] P. Rowghanian, A. Y. Grosberg, *Phys. Rev. E* **2013**, *87*, 042723.

[136] U. F. Keyser, D. Krapf, B. N. Koeleman, R. M. M. Smeets, N. H. Dekker, C. Dekker, *Nano Lett.* **2005**, *5*, 2253.

[137] J. A. Schuller, E. S. Barnard, W. Cai, Y. C. Jun, J. S. White, M. L. Brongersma, *Nat. Mater.* **2010**, *9*, 193.

[138] C. R. Crick, P. Albella, B. Ng, A. P. Ivanov, T. Roschuk, M. P. Cecchini, F. Bresme, S. A. Maier, J. B. Edel, *Nano Lett.* **2015**, *15*, 553.

[139] Y. Li, C. Chen, S. Kerman, P. Neutens, L. Lagae, G. Groeseneken, T. Stakenborg, P. Van Dorpe, *Nano Lett.* **2013**, *13*, 1724.

[140] F. Nicoli, D. V. Verschueren, M. Klein, C. Dekker, M. P. Jonsson, *Nano Lett.* **2014**, *14*, 6917.

[141] N. Di Fiori, A. H. Squires, D. Bar, T. Gilboa, T. D. Moustakas, A. Meller, *Nat. Nanotechnol.* **2013**, *8*, 946.

[142] S. Duhr, D. Braun, *Proc. Natl. Acad. Sci. USA* **2006**, *103*, 19678.

[143] Y. Shangjiong, S. M. Dammer, N. Bremond, H. J. W. Zandvliet, E. S. Kooij, D. Lohse, *Langmuir* **2007**, *23*, 7072.

[144] H. W. Zandbergen, C. Dekker, P. Van Dorpe, M. P. Jonsson, Y. Li, F. Nicoli, C. Chen, L. Lagae, G. Groeseneken, T. Stakenborg, H. W. Zandbergen, C. Dekker, P. Van Dorpe, M. P. Jonsson, *Nano Lett.* **2015**, *15*, 776.

[145] C. Vietz, I. Kaminska, M. Sanz Paz, P. Tinnefeld, G. P. Acuna, *ACS Nano* **2017**, *11*, 4969.

[146] U. F. Keyser, *Nat. Nanotechnol.* **2016**, *11*, 106.